MODELING THE BASIC RING STRUCTURES IN ELEMENTARY PARTICLES OF MATTER

MULTILEVELED CURL ARCHITECTURES AND MODEL DESIGN

Pavel Werner

1   Content

Abstract

The standard model of the universe, its origins, and the structure of matter was formulated during the 20th century [1], [2], incorporating the fundamental theories proposed by the ancient Greek philosophers who recognized the atom as the smallest, indivisible material unit and paved the way to the later adoption of the sphere as the elementary particle [3] of the atomic nucleus and electron cloud. Within this traditional model, however, such particles, defined also quantum mechanically [4], [5], cannot be employed in a convenient manner to provide an adequately accurate explanation of diverse effects of modern physics and chemistry, especially in the context of the state-of-the-art measuring and imaging technologies [6], [7].

Based on available measurements and methods and by posing suitable questions, including how to interpret an electric current below 0.1 aA (attoampere), it appears sufficient to admit that an electron and a quark are subdivisible, leading to the problem of understanding the structure of the sphere [8], [9]. In this context, a spherical body or point may be substituted with another basic geometry - a ring (toroid), for example. This procedure opens the path to a further structural interpretation of matter, a concept where the atomic nucleus has a structure that determines the form of the atom and where the electrons do not move in probability orbitals but levitate at particular (predetermined) spots given by the structure of the nucleus and the balance of the electromagnetic forces. The different view of the topology and structure, whose elementary definition does not require complex mathematics, will render the structure of matter easier to comprehend and imagine. The mathematical simulations (models) and their use will become simpler and less time-intensive, enabling us to explain in a novel manner the physical and chemical effects or processes unrepresentable via the standard model.

The proposed approach embodies an attempt to enhance the description and/or understanding of those effects within elementary particle physics and atomic structure that have hitherto been difficult to clarify. Being an instrument to help reassess relevant problems, the concept enables us to not only explain the basic chemical and physical reasons for the stability and reactivity of atoms and molecules [10] but also discover unknown connections between diverse principles and processes.

1   INTRODUCTION

The designed structural approach utilizes a toroidal object (ring) as the basic component, exploiting also the object's geometrical subset with structural grouping. The underlying ideas, fundamentally systematized and formulated by Pavel Ošmera et al. [11], [12], [13], will be denoted herein as *ring theory* (RT). Interestingly, the theory offers the reader an alternative, viable interpretation of the evolutionary processes that shaped physical science and the inanimate segment of nature in general. By using ring substructures and the standard theories of the electromagnetic field, curl field, and multileveled structures, it is possible to easily characterize and develop relevant models, from those of quantum foam, quarks, the electron, photon, proton, neutron, atoms, and molecules to models of complex organic compounds.

1.1   BASIC PROPERTIES OF THE TOROID

A parametric description of the toroid provides a very effective tool for the model-based expression of the relationships between specific domains of matter; in this respect, the fundamental properties of and concepts relating to the toroidal object are outlined within research report [14]. According to appropriate conclusions [14], the coordinates x, y, z are expressed on the surfaces of the toroid (Fig. 1) via the explicit notation

$$x = x_o + \left(R_1 + R_2 \cdot cos\left(\vartheta\right)\right) \cdot cos\left(\varphi\right),$$

$$y = y_o + \left(R_1 + R_2 \cdot cos\left(\vartheta\right)\right) \cdot sin\left(\varphi\right),$$

$$z = z_o + \left(R_1 + R_2 \cdot sin\left(\vartheta\right)\right), \tag{1}$$

where R_1 is the radius towards the center of the toroid (Fig. 1); R_2 denotes the radius of the toroidal cylindrical surface; x_o, y_o, and z_o represent the coordinates of the toroidal surface center with respect to the origin o of the Cartesian coordinate system; and variables ϑ, φ are the angular local coordinates determining a point on the toroidal surface, which take the values

$$\vartheta \in \langle 0, 2k\pi \rangle, k = 1,...,n, \tag{2}$$

$$\varphi \in \langle -\pi, \pi \rangle, \ R_{1,2} \in \langle 0, \infty \rangle,$$

where n is an integer and defines the relationship between the position of a point on the surface of the toroid in the direction of ϑ and φ.
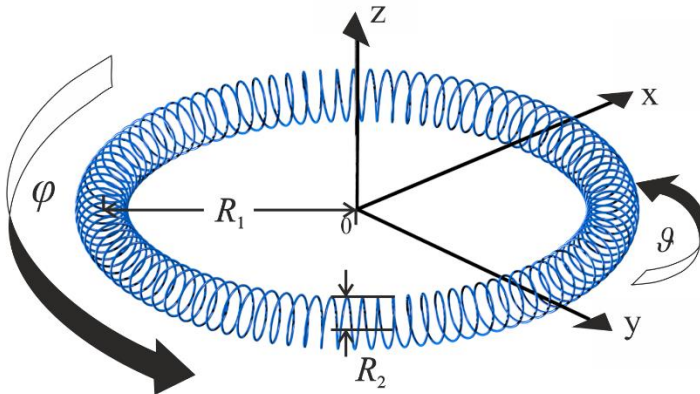

Fig. 1 The orientation of the coordinates and parameters of the basic toroid.

Selecting suitable parameters R_1, R_2, ϑ, and φ allows us to show that, in limit cases, the toroid is capable of assuming the shapes of a sphere, line, circle, point, or another known geometric form.

Where the ratio R_1/R_2 decreases below 1, the trajectory of a point on the surface of a body having such a setting will follow the indication in Fig. 2. In limit states with, for example, $R_1=\to 0$, the resulting object rests in the surface of a sphere, as easily demonstrable by these formulas (1):

$$\lim_{R_1 \to 0}\left\{x_o + \left(R_1 + R_2 \cdot \cos(\vartheta)\right) \cdot \cos(\varphi)\right\} = x_o + R_2 \cdot \cos(\vartheta) \cdot \cos(\varphi),$$

$$\lim_{R_1 \to 0}\left\{y_o + \left(R_1 + R_2 \cdot \cos(\vartheta)\right) \cdot \sin(\varphi)\right\} = y_o + R_2 \cdot \cos(\vartheta) \cdot \sin(\varphi),$$

$$\lim_{R_1 \to 0}\left\{z_o + \left(R_1 + R_2 \cdot \sin(\vartheta)\right)\right\} = z_o + R_2 \cdot \sin(\vartheta) \tag{3}$$

The explicit expression of the coordinates of a point on the toroidal surface in the Cartesian coordinate system, o, x, y, z, can then be written as

$$x = x_o + R_2 \cdot \cos(\vartheta) \cdot \cos(\varphi),$$

$$y = y_o + R_2 \cdot \cos(\vartheta) \cdot \sin(\varphi),$$

$$z = z_o + R_2 \cdot \sin(\vartheta), \tag{4}$$

which corresponds to the notation of the explicitly expressed position of a point on the sphere (Fig. 2) in the Cartesian coordinate system. Assuming a case where $R_1=\to 0$ and $R_2=\to 0$, the resulting object is a point with the coordinates $x_o, y_o, z_o,$ namely, a dimensionless shape; this is demonstrable via transforming formula (1) into

$$\lim_{R_1 \to 0, R_2 \to 0}\left\{x_o + \left(R_1 + R_2 \cdot \cos(\vartheta)\right) \cdot \cos(\varphi)\right\} = x_o,$$

$$\lim_{R_1 \to 0, R_2 \to 0}\left\{y_o + \left(R_1 + R_2 \cdot \cos(\vartheta)\right) \cdot \sin(\varphi)\right\} = y_o,$$

$$\lim_{R_1 \to 0, R_2 \to 0}\left\{z_o + \left(R_1 + R_2 \cdot \sin(\vartheta)\right)\right\} = z_o. \tag{5}$$
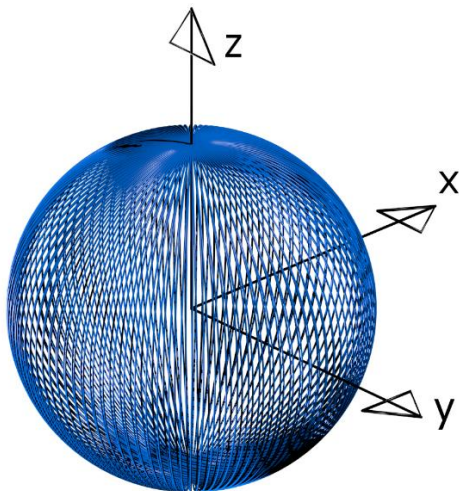

Fig. 2 The trajectory of a point's motion along the basic toroidal surface, $R_1=0.01$, $R_2=1$, at the ratio of $\varphi / \vartheta =100$.

The problem can be further reflected on as proposed by the author of [14].

1.2 MAIN DIFFERENCES BETWEEN THE STANDARD MODEL AND RT

1.   The first aspect distinguishing RT from the classic quantum mechanical theory, which exploits the geometric concept of the sphere as the basic object and relies on Bohr's model of the hydrogen atom, lies in the possibility of endowing a described object with a simple structure and also in the ability to ensure transition/motion at the scale of geometric interpretation. The novel characterization of the basic object arises from the ring (toroid) being a rather general shape and an easily modifiable structure (convenient for simulating shapes such as a sphere (4), circle, point (5), or line, [14]); further in this context, the ring has parametrically modifiable properties and finds use in topological transformations, parametric modeling, structural models whose scale can be changed by orders or magnitude, and other operations or projects. Any such ring (1) consists of toroidal substructures (1) mutually coupled by an electromagnetic field that is generated through the motion of an electric charge q along the surface of the toroid, Fig. 3.
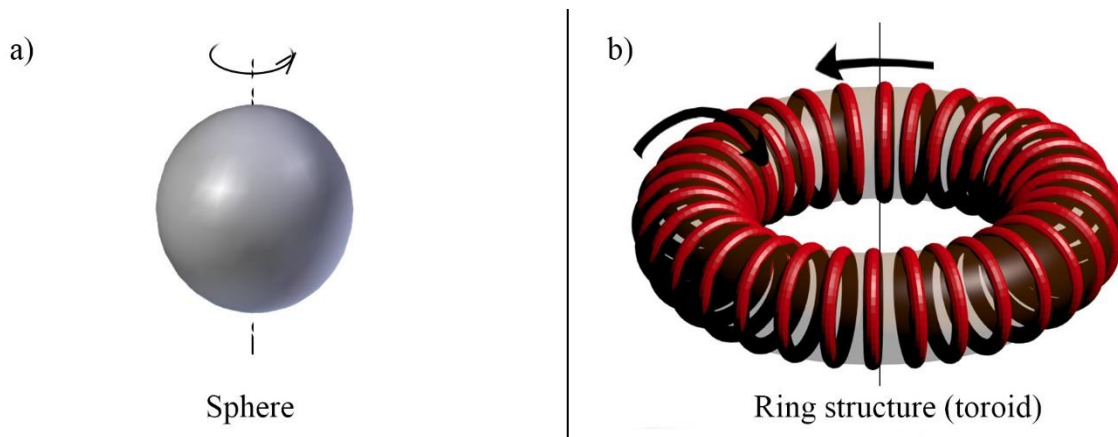

Fig. 3 The basic element of the structure of matter: a) the classic (spherical) concept; b) the toroidal structure to enable the modeling of a fundamental particle.

2.   The second aspect of difference relates to the structure of the atomic nucleus. The nucleus comprises toroidal objects (or structures, (1)), namely, protons and neutrons, which group into between two and five pairs to form a larger cluster. This structuring then exerts a decisive impact on the distribution of electrons in the cloud, Fig. 4.
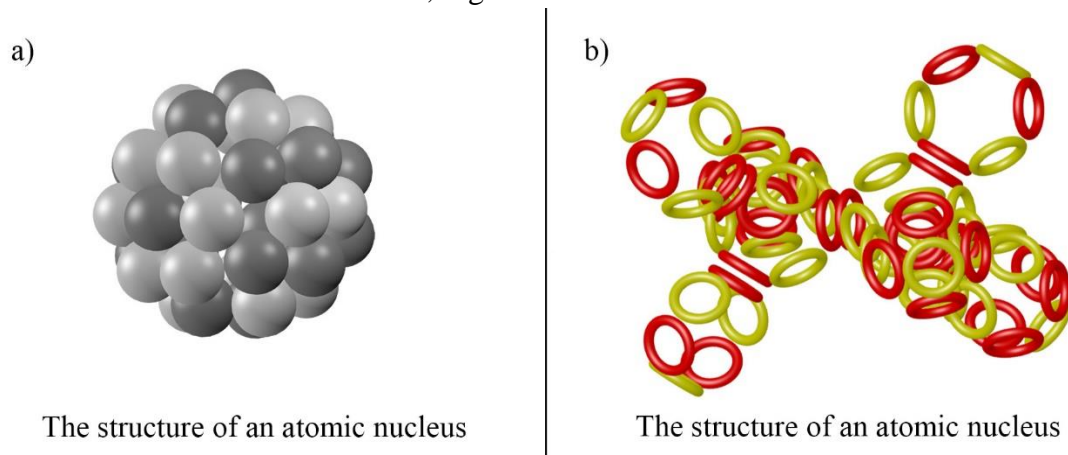

Fig. 4 The atomic nucleus geometries: a) the classic concept; b) the RT-based toroidal interpretation.

3.   The third aspect concerns the position of an electron towards a proton or the nucleus. While

the classic concept exploits a macromodel (such as the planetary model of the solar system), Fig. 5a, the proposed novel view of the structural configuration (Fig. 5b) is based on a levitation model. The electric fields of the positive proton and the negative electron, modeled by using the structure from the corresponding formula (1), cause mutual action of forces. The simultaneously rotating electric charges q of the electron and proton models (1) create magnetic fields, which again interact with each other, and the electric and the magnetic fields – assuming normal circumstances and state of the modeled system, or atom – remain in dynamic balance. In the proposed model of elementary structures, an electron, modeled via the above structure (1), thus does not revolve around the nucleus (Fig. 5b) but remains/levitates at a distance d defined by the balance of the electromagnetic forces. Hence, the balance is formed by the attractive and repulsive forces of the electric and the magnetic fields, respectively, of the electron and the proton; in this context, the actual formation process exploits the relationships between the fields and the electric charge q on the surface of the toroid (1). The distance d is a parameter in the space determined by the axis of the proton-electron rings. The location of the electron with respect to the atomic nucleus is thus specifiable and calculable significantly more accurately than possible via the model characterized and set up by using the planetary system shown in Figs. 3 and 5a).
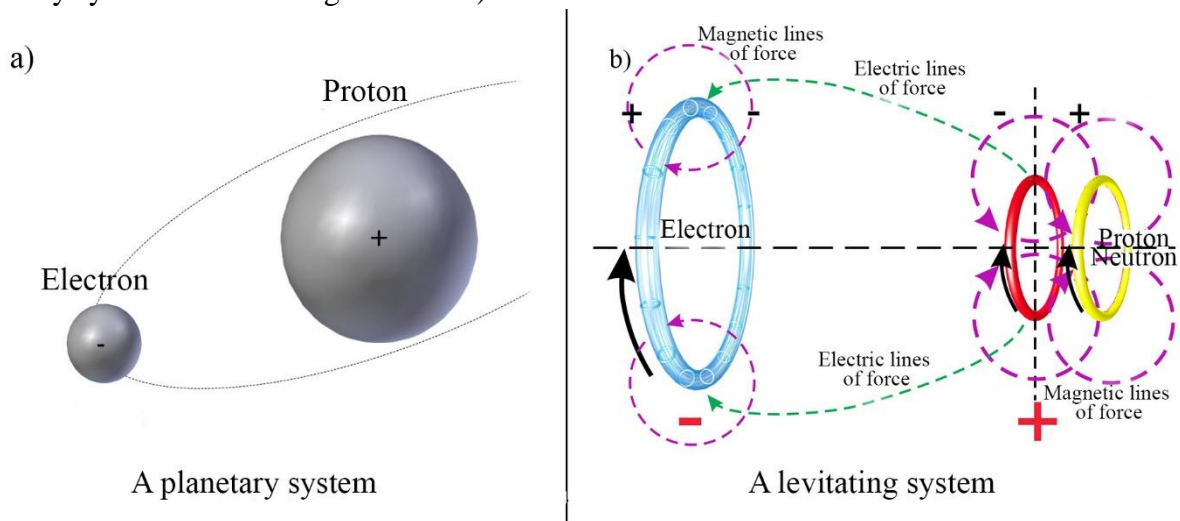

Fig. 5 The classic electron-proton model, a); the novel concept and simulation of the electron-proton particle structure, b).

4

2 MODELS OF THE PROTON AND THE NEUTRON

When modeling a multileveled structure in electrons [13], according to the above-outlined formula (1) and substructural approaches [9], we can assume a similar model in quarks, relying on the same basic toroidal components (1) to form the ring substructures (Fig. 6).

The model of the thermonuclear fusion in the Sun and other stars indicates that the fusion of hydrogen nuclei yields the deuteron and releases the positron and the neutrino; at the advanced stages, the process involves the absorption of electrons during helium nuclei formation and also the generation of neutrons in an alpha particle.

It is thus possible to hypothesize that the structures and substructures of the modeled positively charged positrons participate in forming the light, or "up", quark. Assuming curl electromagnetic fields around the substructures, a geometry change will occur on the long circumference of the ring, namely, this part of the structure will twist into a closed helix maintaining its shape through the neutrinos' force. Similarly, we can adopt the hypothesis that the structures and substructures of the modeled negatively charged electrons contribute to the formation of the heavier, or "down", quark.

Considering the weight of the heavier quark is almost twice that of the "up" one, there arises the assumption that the "down" quark comprises two lighter components coupled to each other by electromagnetic forces. The structural configuration of these parts (Fig. 6), however, creates rather weak coupling, which can be loosened by a comparatively small (also called *weak nuclear*) force.

The higher experimental weight values (m_q) in the quarks, compared to those in the positron and the electron, are ascribable to the structure of the helices. The "up" quarks exhibit a lower weight $m_{q,up}$, meaning that their structure (namely, the helix) in the model is coiled at a smaller angle, or 60°. The heavier, "down", quarks are modeled with the coils angled at 30°, in a direction opposite to that used in the "up" model. Such a choice of angles influences the interaction of the electric fields adjacent to opposing threads and thus also the resulting magnitude of the electric charge (q_q) of the modeled quark. The "up" models then have 2/3 of the resulting positive electric charge q_q, whereas the "down" ones possess only 1/3 of the total value of the negative electric charge q_q (Figs. 7 and 8).
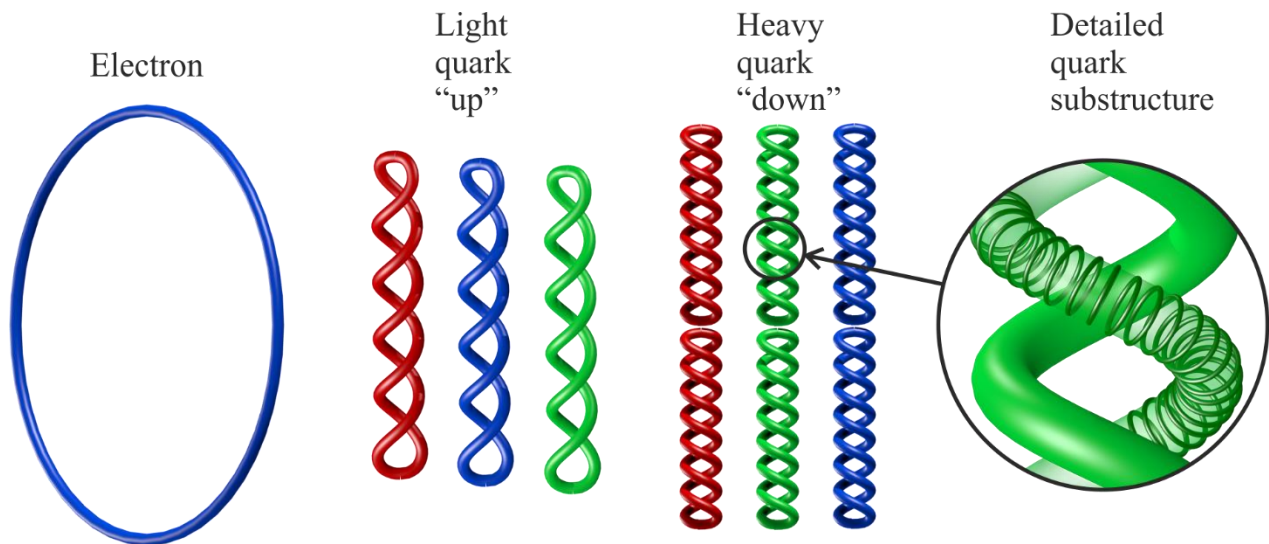

Fig. 6 The "up" and "down" quark shapes and structures simulated via the basic toroidal element.
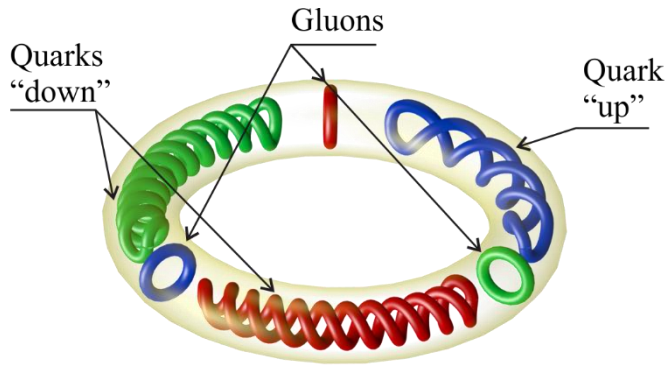
Fig. 7 The "udd" quarks, bound inside a neutron through the force of gluons.
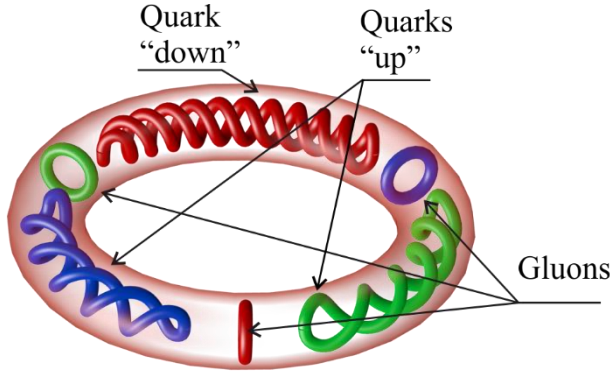

Fig. 8 The "uud" quarks, encased inside a proton through the force of gluons.

The resulting electric charge of the quark, $q_q(t)$, can be modeled as a time-varying, rotating charge which creates the ring structure of the proton and the neutron (Fig. 8). The gluons not only couple the above quark models to each other but also simulate the energy transfer in a manner that ensures energy balance in the entire proton or neutron. In the model, the color-defined properties of the quarks and gluons, hereafter termed *colors* (red, green, blue), invariably coalesce into neutral white (Fig. 9).
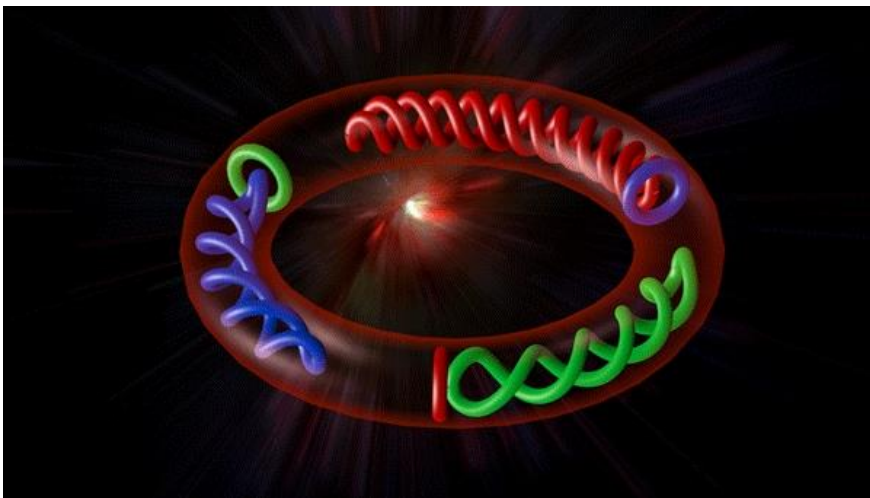
Fig. 9 The exchange of colors between the quarks and gluons of the analyzed proton.

An animation of the color exchange process in the quarks and gluons is available from reference [20].

The coupling between the quarks inside the proton and the neutron is generally mediated by strong nuclear forces; within the proposed RT model, however, the impact of such forces is observable between not only the protons and neutrons having parallel spins on the common axis but

6

also those with antiparallel spins on axes inclined by 60° (Fig. 10). When coupled in this manner, the proton and the neutron form spatial globules and constitute the bases of the nuclear structures of individual elements (Fig. 11).
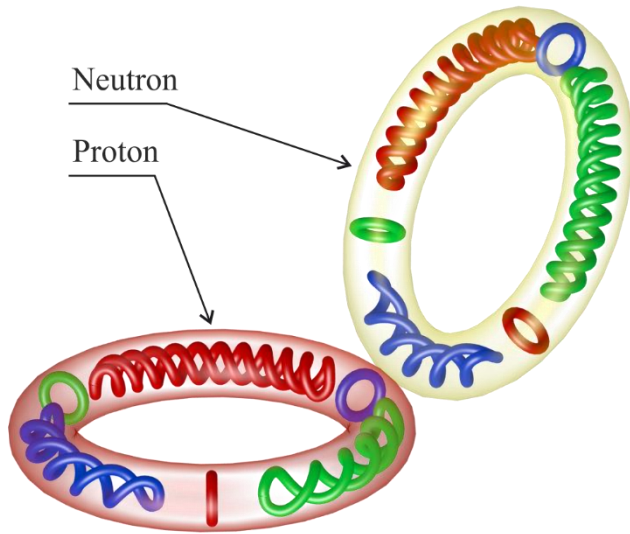

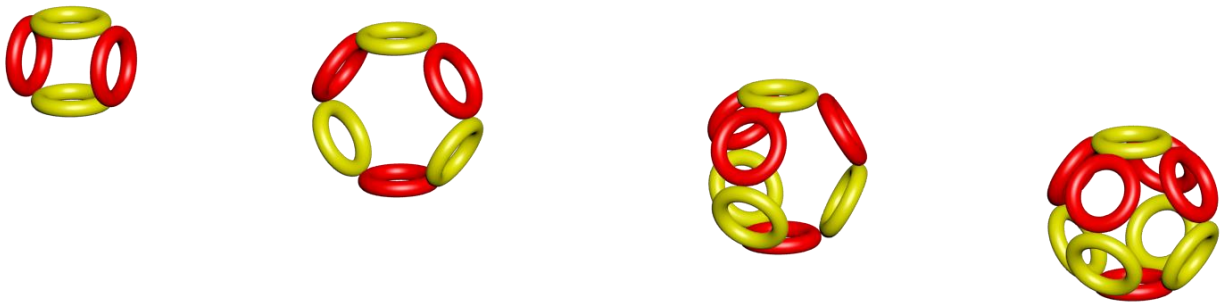
Fig. 10 The proton-to-neutron coupling.

Fig. 11 The modeled basic components of the nuclei of selected elements.

7

3 MODELING THE STRUCTURES OF ATOMIC NUCLEI

In terms of the overall initial conditions to support the modeling procedures, it is possible to assume and then hypothesize that the properties of atoms and the configuration of electrons in the electron cloud are largely predetermined by the structures of the actual atomic nuclei of the elements within the periodic table. Importantly in this regard, the RT-based solution enables us to define the arrangement of the nuclei (visualized above) and thus also to establish more accurately the spatial position of the coupling components, namely, electrons at particular energy levels; such a capability then eliminates the disadvantages of the standard probabilistic model, which does not allow deterministic description and explicit specification of the nuclear structures.

The designed model represents the nuclei by exploiting ring protons and neutrons, as follows:
1. Not more than two protons with parallel spins are coupleable on a common axis.
2. Protons and neutrons having parallel spins are coupleable on a common axis.
3. Two protons with different axes can be coupled through a neutron.
4. Another one or two neutrons can fill the space between two parallel protons.

These four basic rules collectively facilitate the generation of very variable to arbitrary structures of the atomic nuclei of the periodic table elements. Structural transformations are then instrumental for explaining diverse effects via simple visual imaging, an approach where complex mathematical methods using the probability calculus and other relevant tools are not indispensable.

The RT-based atomic nucleus model does not arrange the nucleons in shells, as is the case of the electrons, but rather forms "globules" containing up to 10 nucleons (Fig. 11), the maximum quantity capable of being held in balance by the short-range nuclear forces within the model. Each nucleon may immediately interact with only a limited number of neighboring nucleons. The nuclear forces exhibit a state of saturation, meaning that they couple together merely a restricted amount of such nucleons; moreover, the forces are spin-dependent, with their magnitudes depending on the angle between the ring planes of both particles. The interaction of two nucleons having parallel spins (the pairs proton-proton and proton-neutron) differs somewhat from that of the antiparallel spin nucleons (proton-neutron).

The globules become progressively occupied by neighboring proton-neutron pairs, whose count gradually increases from 3 to 5, to merge into more sophisticated units over proton bridges (proton-proton). Using the globules, we can then express in an ascending order of complexity the RT-modeled nuclei possessed by the individual periodic table elements (according to the quantities of the protons and neutrons).

The globules are shaped by the repulsive electric forces of the positively charged protons and the attractive magnetic forces of the protons' and the neighboring neutrons' magnetic fields (see, for example, Fig. 12). The neutrons in the RT-based model have spins opposite with respect to the protons and thus also exhibit an identical magnetic field direction at the point of contact, namely, they attract each other and maintain the globules in a state of balance (Figs. 13, 14).
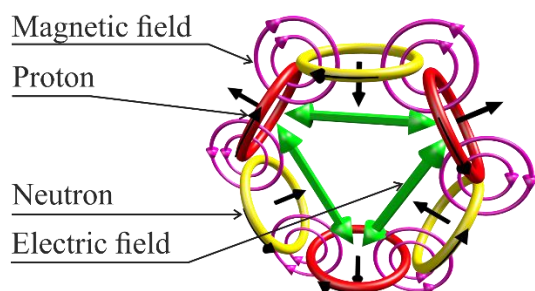

Fig. 12 The lines of force, electric repulsive, and magnetic attractive forces in a nuclear globule (RT).
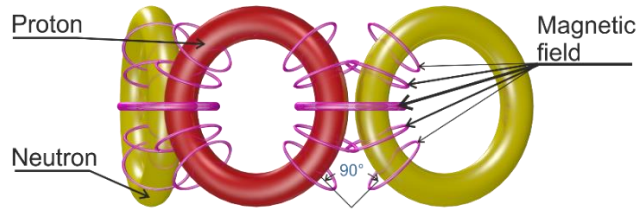
Fig. 13 The magnetic field between a proton and a neutron (RT).

The ring protons and neutrons are mutually coupled by an electric field generated through the rotation of the relevant electric charges of the quarks (q_q) inside the rings. As the protons and neutrons in a globule have oppositely oriented magnetic moments, their magnetic fields superpose in the region of approach and, as a result, attract each other; the area of such attraction, however, encompasses only a quarter of the fields' perimeters, considering the ring structure of the globules. If the angle between the ring planes equals approximately 120°, the magnetic fields are perpendicular to each other; at 45°, their strengths begin to decrease rapidly, even down to zero (Fig. 13), and the nuclear forces are thus defined as short-range.

In these aspects, the RT-based model corresponds to the experiments performed so far [8], enabling us to assume that, within the proton and neutron ring structures, there is no special "strong nuclear force" but rather only a standard, firm magnetic force.

The globules may couple as demonstrated by the "proton bridges" model in Fig. 14.
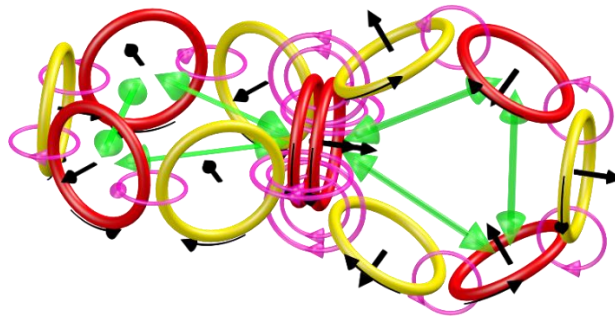
Fig. 14 The "proton bridges" globule coupling concept.

The models representing the isotopes of the elements of the periodic table exhibit also rising numbers of the nuclear neutrons, which either are located between two protons or form the proton skin of the remotest globules. Such a configuration then results in an increased mutual repulsive magnetic force with respect to the electrons and, simultaneously, yields an isotope's radius larger than that comprised in the model of the same element in the basic state (Fig. 15).

C_{12} C_{13} C_{14}

Fig. 14 The carbon isotopes' nuclei.

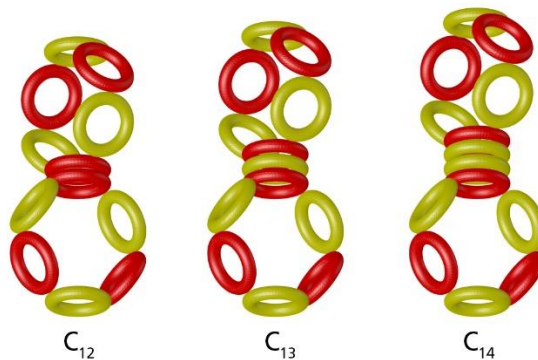The globule-based nuclei may take the shapes of not only a sphere but also a flattened (carbon) or prolate (many other nuclei) ellipsoid or other, more complex geometric formations. The shapes of some atomic nuclei within the periodic table of elements may exist in multiple modifications (allotropic structures).

Neighboring globules influence one another by means of their magnetic fields, depending on the number of a globule's nuclides and their mutual positions; this interaction manifests itself through shape deformation towards the proton coupling site at the center of a globule (Fig. 16). In the modeled ring structures, a rise in the magnetic field inhomogeneity increases the intensity of the resulting coupled field and thus also the force, meaning that the part of the ring that lies somewhat farther away from the ring's axis is acted upon by a greater force, Figs. 16 to 18. Advantageously, the deformations allow us to clarify smoothly the known coupling angles in carbon, nitrogen, and oxygen, and they also affect the arrangement of the molecules and the actual crystal lattice shapes.
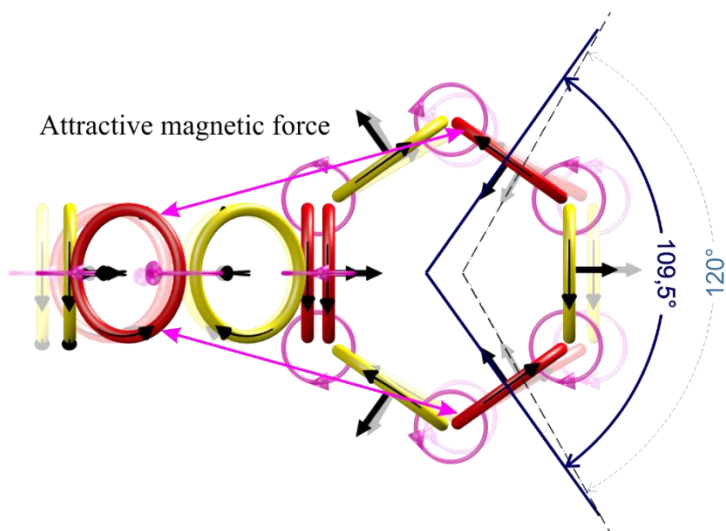

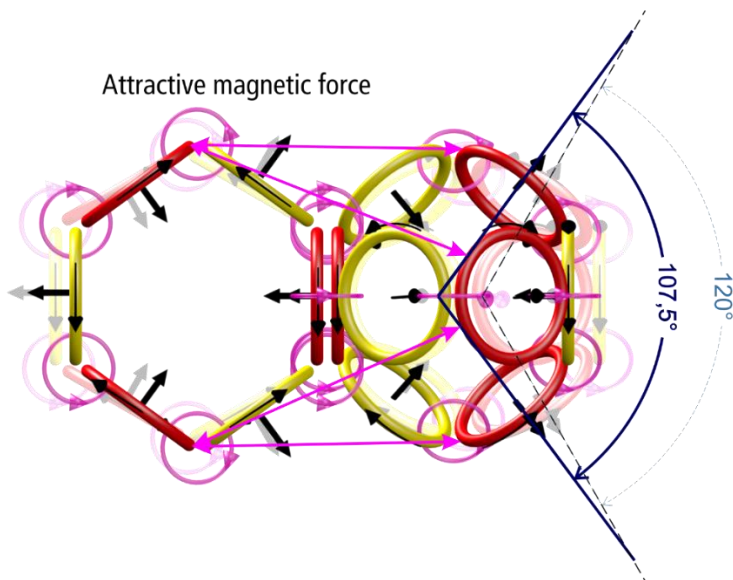**Fig. 15** The carbon nucleus globules deformed by a force F_{mag}.

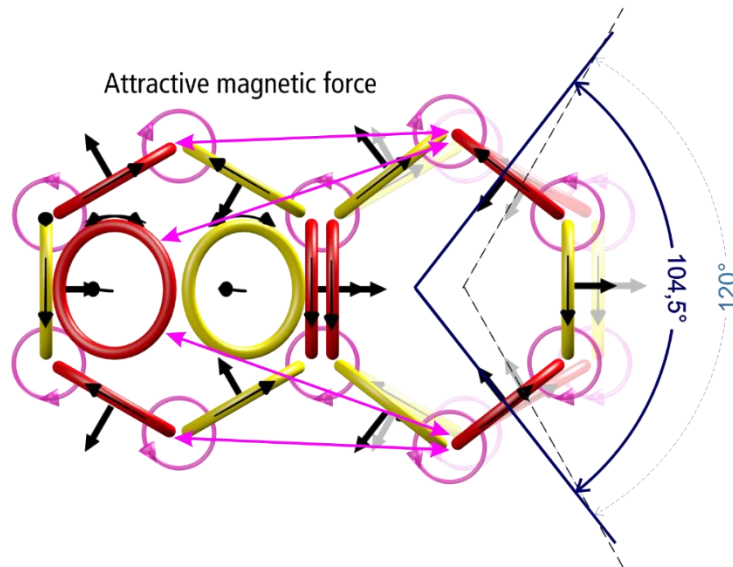**Fig. 16** The deformation of the globules in the nitrogen nucleus.

Fig. 17 The deformation of the globules in oxygen; the magnetic forces' F_{mag} orientation and distribution.

The strong, electromagnetic, and other (weak) interactions predetermine the energy conditions in the nuclei according to the relationships between and configuration of the protons and neutrons. The nucleons parametrically express and enter certain quantum states (Fig. 19), or energy levels, to create globules, and they emit gamma radiation photons when transiting between the states. The individual levels fill with the protons and neutrons gradually, respecting the progressive formation of the nuclei of the elements of the periodic table (from the simplest items up to the given element).
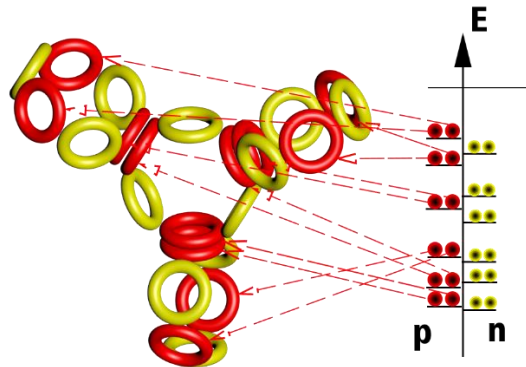

Fig. 18 The coupling energy of the protons and neutrons in the magnesium nucleus (Mg).

The globules containing the highest sum of the nucleons (five proton-neutron pairs) constitute an exceptionally stable portion of the nucleus, by analogy with an atom exhibiting completely filled electron levels.

Particularly stable are those nuclei in which the count of the protons and neutrons is characterized by the numerical series 2, 8, 20, 28, 50, 82, 126; these RT-based nuclei have a symmetrical arrangement and possess globules filled with the maximum possible quantity of the nucleons.

The nucleons in a modeled atomic nucleus are not static but have their own internal spins, and also the quarks and gluons rotate along the axes of their toroids. These rotations are coupled to the neighboring nucleons through components of the electric and the magnetic fields to produce deterministically and explicitly defined couplings; moreover, the rotations can be described at any time, similarly to the well-known automobile transmission system. In the model, the spins of opposing nucleons indicate whether the energy flux of the coupling elements, namely, the toroids representing

the electrons, is directed towards or away from the globule (Fig. 20), and this property then specifies the type of spin proper to the electron that couples with the pair proton – neutron.
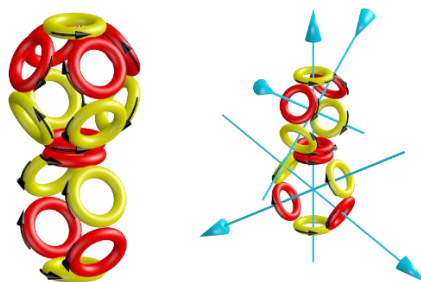
Fig. 19 The rotation of the oxygen nucleons, and the directions of the magnetic moments in the carbon nucleus.

Those of the modeled elements that have similar external structures of the nucleus (Fig. 21) exhibit also comparable properties.

6	15,99
Carbon	
C	2,5
$2s^2 2p^2$	
14	32,06
Silicon	
Si	1,7
$3s^2 3p^2$	
32	72,61
Germanium	
Ge	2,02
$3d^{10} 4s^2 4p^2$	
50	118,71
Tin	
Sn	1,72
$4d^{10} 5s^2 5p^2$	
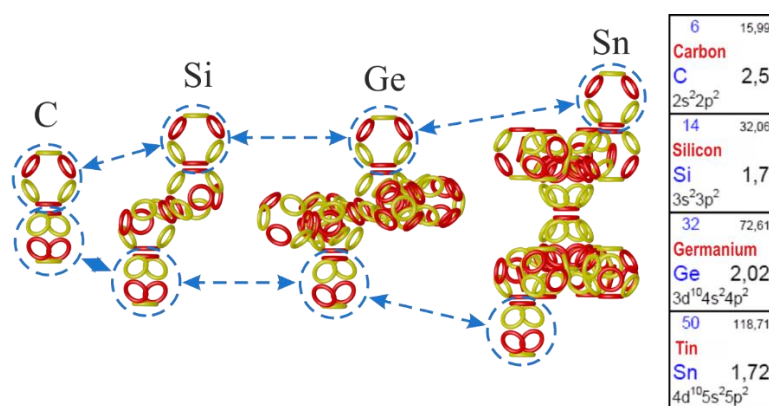
Fig. 20 The comparable nuclear structures of C, Si, Ge, and Sn.

The atomic nucleus structure modeled by using 3, 4, and 5 proton globules exerts influence on the ionization energy of atoms having such a composition; thus, each major change of the nuclear structure will show itself through an alteration in the corresponding atoms' ionization pattern (Figs. 22, 23, and 24).

Fig. 21 The ionization energy W of the modeled atoms.

12

Fig. 22 The RT-based atomic nuclei structures.

Li	Be			B	C	N	O	F	Ne
3	4			3	3	3	3	4	5
2				2	3	4	5	5	5

Na	Mg			Al	Si	P	S	Cl	Ar
3 5	4 5			3 5	3 5	4 5	3 - 5	4 - 5	5 - 5
3	3			3	3	3	4	4	4
				2	3	3	4	4	4

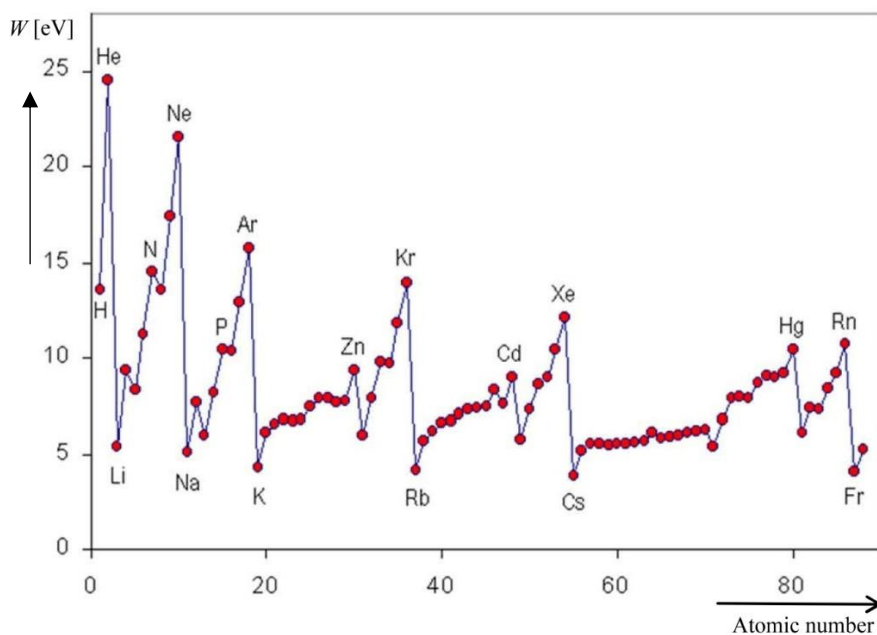| K	Ca	Sc		Ga	Ge	As	Se	Br	Kr
4 − 4	3 − 3	3 − 4		3 3 4	3 3 5	3 4 5	3 4 5	4 4 5	4 5 5
4	4	4		4	4	4	4	4	4
4	4	4		4	4	4	4	4	4
- 3 -	3 - 3	3 - 3		3 5 5	3 5 5	3 5 5	4 5 5	4 5 5	4 5 5

	Ti	V	Cr	Mn	Fe	Co	Ni	Cu	Zn
	3 − 4	3 − 4	4 − 4	4 − 4	4 − 5	4 − 5	5 − 5	4 − 4	3 3 3
	4	4	4	4	4	4	4	4	4
	4	4	4	4	4	4	4	4	4
	3 − 4	4 - 4	4 - 4	4 - 5	4 - 5	5 - 5	5 - 5	3 5 5	3 5 5

Rb	Sr	Y		In	Sn	Sb	Te	I	Xe
				3	3	3	3	3	3
3334	3335	3335		3335	3345	3355	3455	3555	4555
5	5	5		5	5	5	5	5	5
5	5	5		5	5	5	5	5	5
3335	3335	3345		4555	4555	4555	4555	4555	4555
				3	3	3	3	3	3

	Zr	Nb	Mo	Tc	Ru	Rh	Pd	Ag	Cd
	3345	3345	3355	3355	3355	3455	4455	4555	4555
	5	5	5	5	5	5	5	5	5
	5	5	5	5	5	5	5	5	5
	3345	3445	3445	3455	4455	4455	4455	4455	4555

Fig. 23 The structures of the globules, with the numbers representing the count of a globule's protons.

4   MODELING THE ELECTRON

In the classic theory of the structure of matter, elementary particles constitute physical objects having an electrical character. The electron is considered a point particle, described parametrically via magnetic properties, and the electric charge carried by an electron (q_e) is assumed to be in motion. Such a concept, however, does not explain the results of experiments in which the electron occurs at different sizes, from 10^{-18} m and 10^{-12} m in the accelerated and coupled variants, respectively, through Rydberg electrons up to 10^{-5} m in the free form.

A viable approach to refining and solving diverse hypotheses and models could eventually consist in the speculation that the electron comprises multiple smaller, modifiable substructures which facilitate a change of its size (Fig. 25). Although current technologies and possibilities do not enable us to reveal the multileveled structures of electrons, this deficiency does not necessarily mean that the arrangement is merely fictitious.
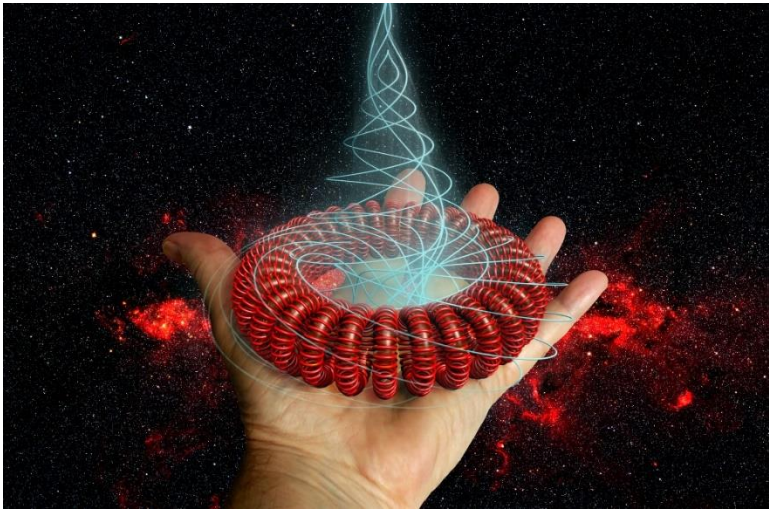

Fig. 24 The electron as interpreted in RT.

Ring theory proposes a model of the electron as a toroid-shaped dynamic particle composed of multileveled (and convenient for submodeling and substructuring), compound ring substructures, mutually coupled by an electromagnetic field.

The modeled substructures (Fig. 26) with dimensions R_1, R_2, R_3… carry negative electric charges q, creating an electromagnetic field around their rings. The rotational motion of the charges q on the substructures generates a field with components that, in the magnetic part, produce a characteristic distribution, similarly to the case of a magnetic dipole. The individual rings of the substructures are repelled by the electric field but attracted by the magnetic one, until balance has been achieved. Such a condition occurs at typical intersubstructural distances and electron sizes.
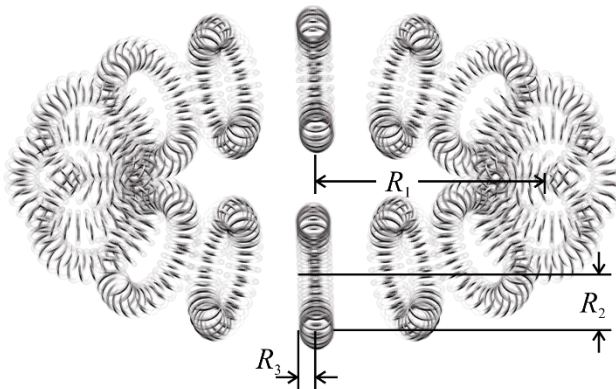

Fig. 25 The basic structure of the electron model.

4.1 QUANTUM NUMBERS

Within RT, the quantum stationary state of the electron in a hydrogen atom is described by four quantum numbers: n, l, m, and m_s.

The primary number, n (Fig. 27), indicates the energy level in the model of the electron; the level is quantized, denotes also the distance of the electron from the center of the atomic nucleus, and takes a value 1, 2, 3, 4, 5… up to infinity. In the presently established theory of the description of matter, the primary number nevertheless takes values in the interval of n=1...7. Upon ionization, namely, when receiving an amount of energy that causes a particle to separate from the structure, an electron becomes free, and its energy ceases to be quantized; the electron thus may acquire an arbitrary volume of positive kinetic energy.
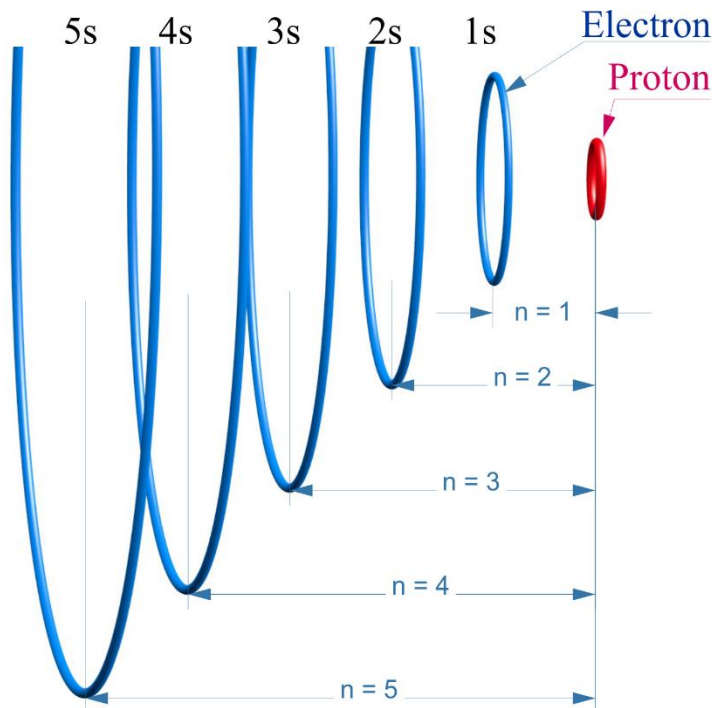

Fig. 26 The quantum number n.

The secondary quantum number, l (Fig. 28), is limited by the value of n and may take a value within l=0, 1, 2, 3, …, (n–1). The l values are assigned letters as follows:

l value   0, 1, 2, 3, …
letter   s, p, d, f, …(g).

In the model, the secondary quantum number indicates the degree of irregularity of an electron's shape; the unique, undulation-like bends illustrated below embody the spiral twisting of the ring structure. The electron substructures turn by l 360°.
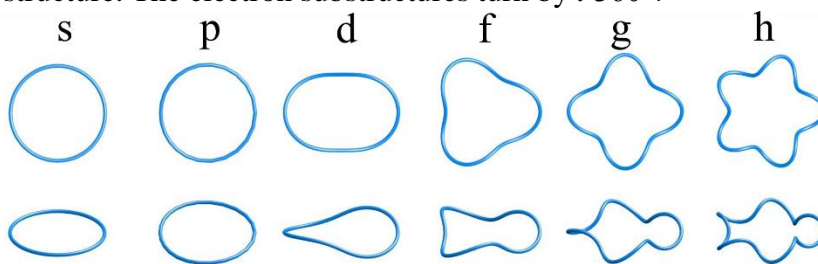

Fig. 27 The quantum number l.

The magnetic quantum number, m (Fig. 29), denotes the quantity of variations of an electron's orientation in space with respect to the atomic nucleus. The m value may change between m $\in$ <-1, +1> (including zero); thus, for example, if l=2, we may adopt a value m= -2, -1, 0, 1, 2:

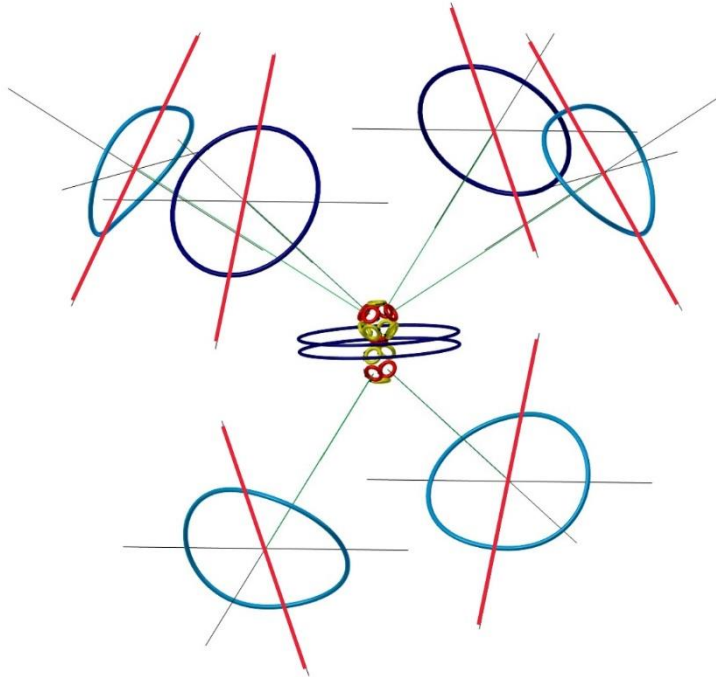|		
s	<0>	1 spatial variation
p	<-1, +1>	3 spatial variations
d	<-2, +2>	5 spatial variations
f	<-3, +3>	7 spatial variations.

Fig. 28 The quantum number m of the spatial orientation of the oxygen atom's electrons.

The standard model, used to date and formulated according to quantum mechanics, proposes that the spin magnetic quantum number, m_s (spin), indicates the electron rotation direction and takes a value $\pm 1/2$. By extension, the model also suggests that a particle's spin can be accurately introduced only via exact computations and formulas based on the quantum mechanical mathematical model.

In the coupled ring model of the electron, however, the spin orientation can be determined. The model carries in its substructures an electric charge q, which, during its motion along the surface of the modeled electron, generates an appropriate magnetic field. Therefore, if the main electric charge moves at a velocity v_0 in the direction of the arrow (Fig. 30) and the associated electric charge on the first level substructure of the toroid progresses at a velocity v_1, also in the direction of the arrow (Fig. 30), then the motion of the electric charge q creates in the ring of the modeled electron an instantaneous value of the electric current $i(t)$ having an amplitude I, and the process follows a direction opposite to that of the electric charge moving at v_0. The passage of the electric current produces a relevant magnetic field, oriented according to the right-hand rule. This magnetic field can be characterized as a magnetic dipole which, similarly to a permanent magnet, exhibits an oriented magnetic moment (Fig. 30). The orientation of the magnetic moment (μ_e) is identical with that of the spin, "S". In the RT-based model, the spin is referred to as the "actual" or "internal" spin, determined by the negative electric charge q and further defined by the direction of the charge's rotation along the surface of the outer ring as well as by the rotation direction of the substructural rings.
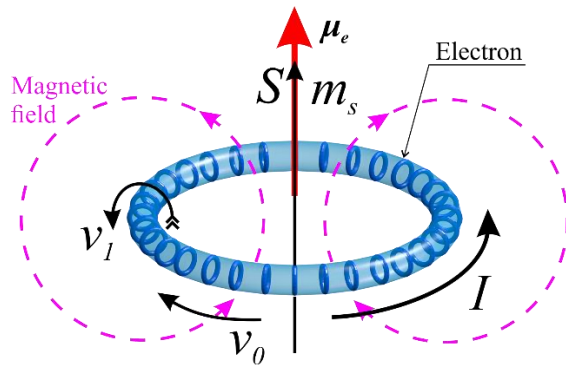
Fig. 29 The electron spin.

If a change occurs in the direction of the motion of either the electron's electric charge q at v_0 (Fig. 31a)) or the electric charge in the substructures at v_1, such a condition will not produce a model of an electron having an opposite spin (m_s) but rather a model of another particle with a positive charge q (positron). The figure below (Fig. 31b)) displays the differences between the negatively charged electron and the positively charged positron or proton.
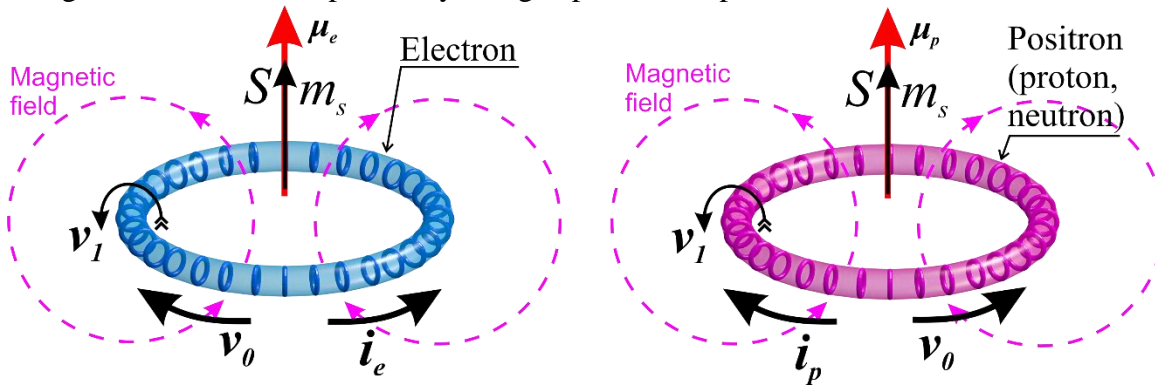

Fig. 30 The spin (m_s) in the electron, a) and the positron, b).

In view of the description, the electron does not possess its own positive or negative spin; instead, it has merely one specific inner spin. Thus, the spin can be characterized as identical, parallel, or antiparallel (namely, "positive" or "negative") only when a particle modeled as shown above has been influenced by or coupled with an external reference magnetic field, another fundamental particle, or an atom nucleus.

The elementary particle models (Fig. 32) having opposite spins (proton – electron) repel each other, based on the orientation of their magnetic fields; conversely, the particles with identically oriented parallel spins (electron – electron) attract each other via their magnetic fields' coupling. Two electrons of two atoms exhibiting the same motion direction at v_0 of the electric charge q and having an identical spatial orientation of the spins m_s will be subjected to mutual influence – upon close approach, through attractive magnetic forces - and may thus produce a model of the known covalent bonding. In the proton and the neutron, an identical rotation orientation of the charges q at v_0 is applied, meaning also application of identical magnetic moments $\boldsymbol{\mu}_p$ and $\boldsymbol{\mu}_n$ as well as spins S_p and S_n.
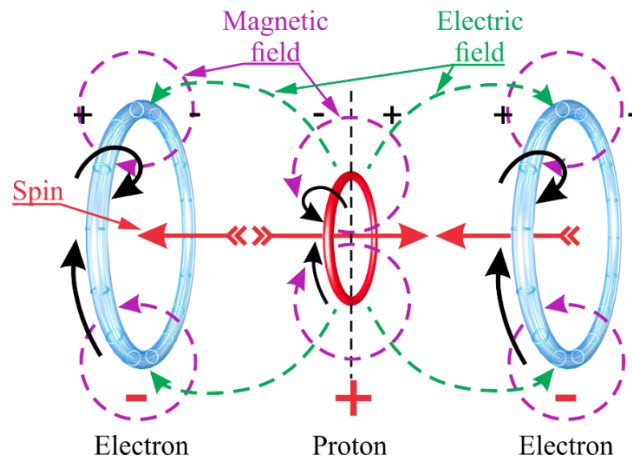
Fig. 31 The oppositely oriented spins (magnetic moments) in the proton – electron coupling.

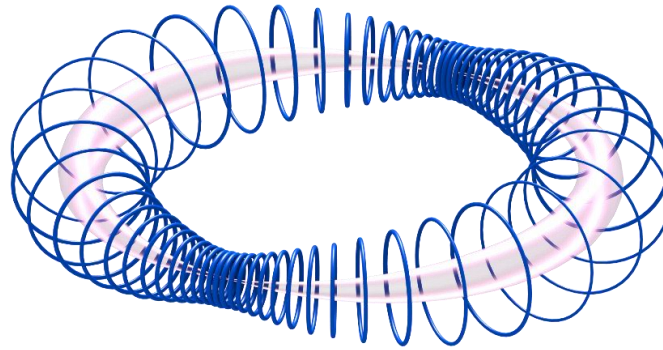## 4.2 SHAPE AND SIZE OF THE ELECTRON IN RT-BASED MODELS

Fig. 32 The dynamic behavior of the modeled electron.

Considering the hitherto characterized experiments, calculations, and theories, it is possible to hypothesize that an electron modeled according to RT constitutes a dynamically composed, toroid-shaped structure comprising multi-level compound structures held together by electromagnetic forces (Fig. 33).

Such an architecture enables the modeled electron to respond via excitation to a variation in its own energy or coupling power. The response will materialize through a change of the model's geometric dimensions, namely, an increase or a decrease of the actual diameter of the ring; in this context, computing a universal size of the electron appears to be only a task of low importance and little meaning. The ring's substructures form a dynamic structure with variable parameters R_1, R_2 (Fig. 1, Fig. 26), and these are defined merely by the amount of the structure's internal energy or coupling potential. With respect to the above assumption, not even the size of an electron on the "*s*" level in the hydrogen atom model can be considered the basic measure, because the "*s*" level electrons in the heavier elements are much closer to the atomic nuclei and have markedly smaller radii, mainly due to the fact that they adjust to the coupling forces to establish balance.

The free electron is modeled as an entity that seeks to change its position and location, namely, to delocalize itself. In the Heisenberg uncertainty formulas, a more delocalized entity exhibits less kinetic energy. The size of the geometric model (Figs. 1 and 26) varies between tens and hundreds of nanometres, and the model is capable of responding to the presence of other bodies via electromagnetic coupling; the effect of a positive particle, for example, will manifest itself within

several picoseconds, allowing the modeled electron to gain a remarkably more compact shape and to alter its geometry, potentially down to a quarter of nanometer in the radius R_1 [15]. Information regarding the geometric dimensions from diverse experimental measurements of the electron can be obtained by utilizing the absorption spectral lines. In the model (Fig. 26), the free electron, if its R_1 is within hundreds of nanometers, emits electromagnetic waves in the corresponding frequency band. Subsequently, the model will respond to a change in the geometric dimensions R_1, R_2, shrink to a smaller size, and irradiate electromagnetic waves from the related frequency band, starting at GHz and progressing through THz and the infrared range to the red band in the visible part of the electromagnetic spectrum. The shrinking of the electron is caused by the electromagnetic forces of the proton(s), above all, in the discussed case, the electric component at the level of the modeled electron's ring. The force induced by the magnetic component has a similar impact, albeit, as indicated by the model, a markedly less intensive one compared to that of the electric field.

The stability of the modeled electron's structure (Fig. 26) depends on the dual motion of the electric charge and the resulting oscillation. In each substructure, such motion involves standing transverse oscillation (expansion and reduction of the radii of substructures R_{1sub}), Fig. 33, and a traveling electromagnetic wave propagating along the perimeters of the ring and its substructures; this wave, upon superposition of the electromagnetic components, causes a phase shift of the standing waves in the substructures. When combined, the two types of waves enable the electric charge to move along the perimeter of the electron. Superposing the waves will generate on the structure of the toroid spots with a "greater" or "smaller" electric charge q, an effect interpretable as an electric dipole; through its temporal distribution on the surface of the main structure of the toroid, the electric charge q forms a corresponding magnetic field. Relative to the global coordinate system, the electron model and its substructures do not move but create an EMG wave.

In 2008, a research team led by F. Barry Dunning of Rice University succeeded in their efforts to graphically represent highly excited potassium atoms [16], [17]. The resulting images were interpreted as containing atoms whose electrons had a highly localized wave function and which exhibited a probability maximum orbiting a circle; these atoms behaved like classic particles, Fig. 34.

With the RT-based approach to elementary particles of matter, the images (Fig. 34) are nevertheless describable also as capturing the electric charge distribution at time moments along the perimeter of the ring structure of the electron model.
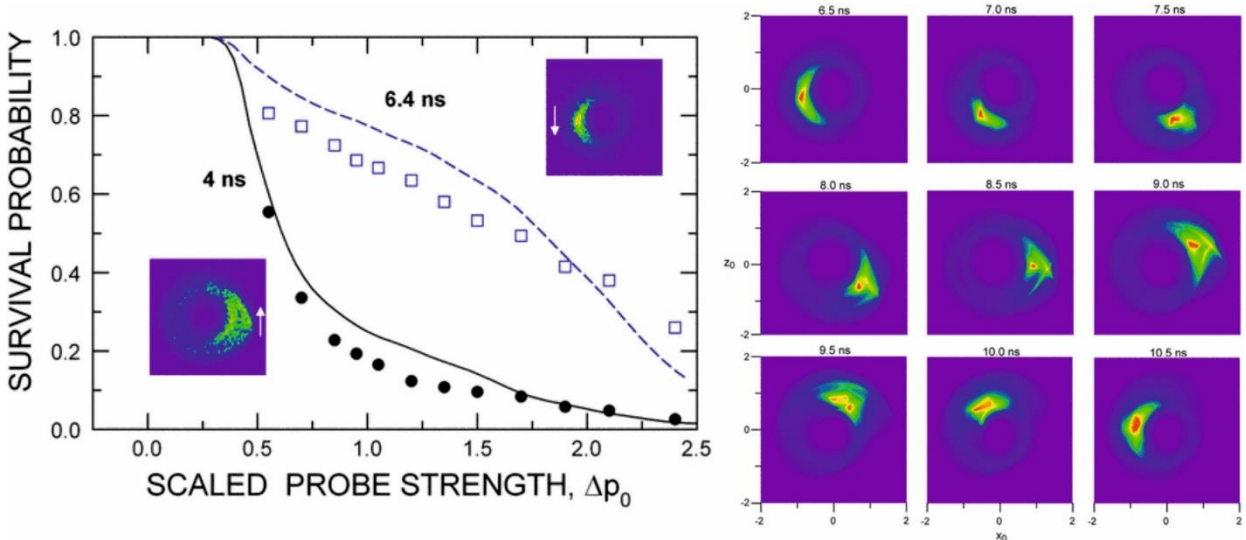

Fig. 33 The localized electron [16], [17],

Within the model, each separate basic element (electron) and its substructures possess their electric and magnetic fields, formed by the instantaneous value of the electric charge $q(t)$. In the axis of the ring, the module of the mean values of the electric field intensities and flux densities then shows

20

a minimum, or zero, value ($R_1=0$), while the mean value of the magnetic intensity or flux density modules reaches the highest magnitude (Fig. 35).
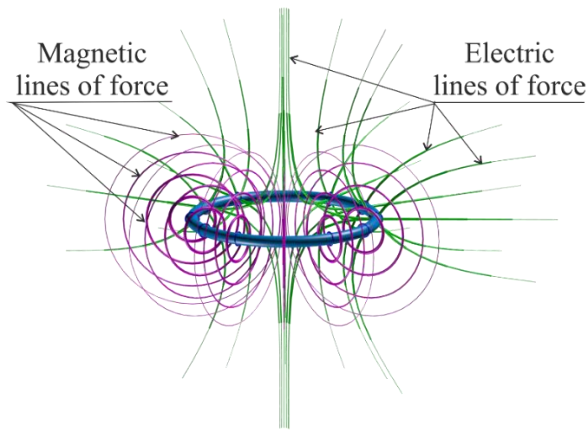

Fig. 34 The distribution of the lines of force relating to the electric and the magnetic fields of the RT electron.

Upon superposition of the electric and the magnetic components of the electromagnetic field, two or more substructures influence one another by means of their electric components; in the process, the substructures are mutually repelled and attracted through the relevant electric forces and magnetic fields, respectively. The superposition of the electromagnetic fields depends on the distances and sizes of the elements in the model; these partial fields then create the resulting field, characterizable by the lines of force, and thus form a system of elements in dynamic balance. Within the assumed limits of the RT-based electron geometry, the forces acting in the model are strong and satisfy the stability requirements placed on the designed structure and substructures (Figs. 36 and 37).
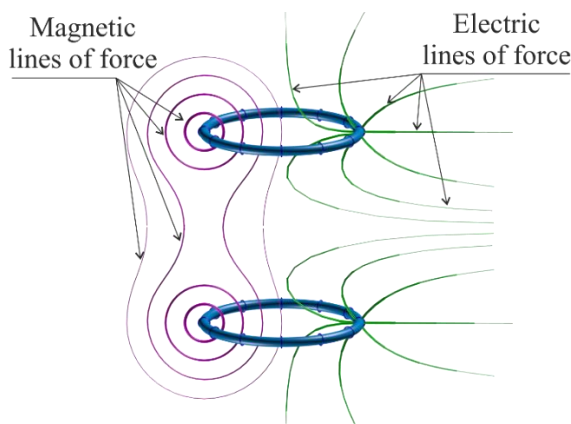

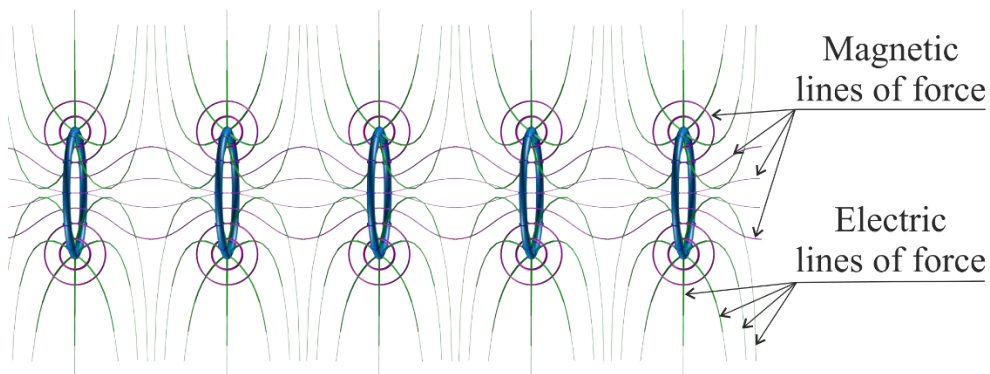**Fig. 35** The inter-element forces from the electric and the magnetic fields of the electron substructures.

Fig. 36 The magnetically coupled electron substructures.

21

In relation to the geometry, namely, the size of the toroid ring radius R_2, we can formulate a hypothesis resembling that applied to the model and size of the quarks. Presuming the quarks also have their substructures and, in the disintegration of a neutron, the heavy quark decays into a light one, an electron, and an antineutrino, it is possible to consider the quark and electron substructures identical and to interpret the electron as only a simpler structure in the more complex architecture of the quark. If, in the context of the above speculation, the size of the quark is within $R_1 = 10^{-18}$ m, then that of its substructures does not exceed $R_{1sub} = 10^{-21}$ m, meaning that the models of the first substructure of the electron belong to the same order of size. However, after being released from the model of the quark, the electron should/might exhibit a size larger by up to 13 orders, and a corresponding increase of geometrical parameters would be expected in its substructures.

In the model of the electron, an increase in the quantum number n is accompanied by absorption of the incident external energy, embodied in, for example, a participating photon. Such energy then causes the number of the nodes, antinodes, and substructures (Fig. 38) to rise n-times; simultaneously, the radius R_1 and the perimeter will increase, too. This higher count of the nodes will not produce an amplified electric charge q but a changed magnetic field of the electron, leading to altered (enhanced) action of the forces; as a result, the modeled electron will move to a position more distant from the atomic nucleus, thus relocating to a higher energy level.
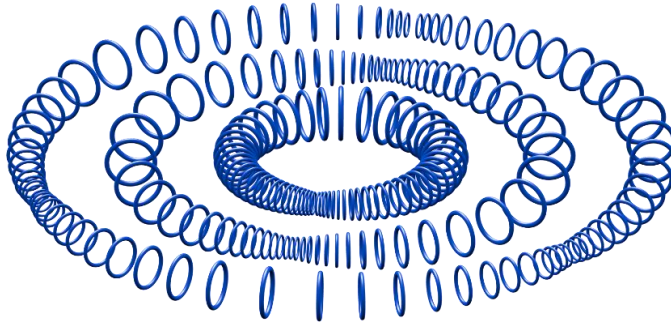

Fig. 37 The amount of antinodes and its growth in response to a rise in the quantum number n.

4.3 CALCULATING THE ELECTRON RADIUS VIA SPECTRAL LINES

To calculate the radius R_1 in the modeled hydrogen atom's electron, we can employ the approach well known from quantum mechanical models of matter, utilizing moments evaluated as the terms of the individual spectral series, namely, the

1. Lyman (ultraviolet part of the spectrum),
$$T_L = 91.1 \cdot 10^{-9} m \quad , \tag{6}$$
2. Balmer (the visible band),
$$T_B = 364.6 \cdot 10^{-9} m \quad , \text{ and} \tag{7}$$
3. Paschen series (the infrared band).
$$T_P = 820.4 \cdot 10^{-9} m \quad . \tag{8}$$

The previously published studies [18] enable us to assume that a model/interpretation of the photon may take the shape of a double loop, and when the photon is released or received by the electron, it has to rotate twice around the electron's perimeter. This process presumably takes place at a speed v lower than the speed of light c. The energy of the photon will split into two halves - one absorbed into the wave and electromagnetic properties (oscillations) of the model, consequently facilitating magnetic field intensification at the first substructural level, and the other distributed among the corresponding lower sublevels. As regards the wavelength and term of the photon, we will divide the latter by four, and the resulting one-fourth portion will then be divided by the perimeter of the electron to yield the inverse value of the constant α, which indicates how many times lower than the speed of light is the speed of a charge moving around the perimeter. We have

$$\frac{T_n}{4} \cdot \frac{1}{2\pi r_e} = 137 ,$$ (9)

$$\frac{1}{\alpha} = 137 ;$$ (10)

it follows from this formula that the radius of the electron, $R_1 = r_e$, is

$$r_{e1} = \frac{T_n \cdot \alpha}{4 \cdot 2\pi \cdot n^2} .$$ (11)

For a hydrogen atom term of the first series, whose wavelength corresponds to $91.2 \cdot 10^{-9}$ m, the radius of an electron on the first orbit is expressed as

$$r_e = \frac{91.2324 \cdot 10^{-9}}{4 \cdot 2\pi \cdot 137 \cdot 1} = 2.65099 \cdot 10^{-11} m .$$ (12)

Regarding the radius of a hydrogen atom electron of the second and third quantum levels ($n=2$ and $n=3$), we have

$$r_{e1} = \frac{T_2 \cdot \alpha}{8\pi \cdot n} = \frac{364.6 \cdot 10^{-9}}{8\pi \cdot 137 \cdot 4} = 26.5 \cdot 10^{-12} m ,$$ (13)

$$r_{e1} = \frac{T_3 \cdot \alpha}{8\pi \cdot n} = \frac{820.4 \cdot 10^{-9}}{8\pi \cdot 137 \cdot 9} = 26.5 \cdot 10^{-12} m .$$ (14)

At the individual quantum levels, the radius of the modeled electron expands n times.

The growth in the number of the nucleons is accompanied by a rise in the nuclear coupling force; as a result, the electrons are drawn closer to the nucleus, and the ionization energy w_{io}, which is required to release the electrons from the atom, increases. According to generally known hypotheses, greater ionization energy means shorter wavelength of the ionization photons; in the designed model, such a relationship corresponds to a smaller radius R_1 in the electrons at the individual energy levels, meaning that an electron on level $1s$ inside the hydrogen atom exhibits a radius R_1 markedly larger than that of an electron occupying the same level in, for example, the iron atom. With decreasing values of radius R_1, the levels progressively approach the atomic nucleus, and therefore the growth in the number of the nucleons reduces the radii R_1 of both the modeled electron and the related atom.

The radii R_1 of the electrons on level $1s$ in selected elements of the periodic table are summarized in Tab. 1 below.

Tab. 1 The atomic electrons' radii R_1 in selected elements

Element	Term 1, T (nm) [27]	Electron radius: level $1s$ R_1(pm)
H	91.2328	26.5
He	50.4577	14.662
C	4.809	0.3493
O	1.46	0.425
Si	0.514	0.149
S	0.369	0.107
Fe	0.139	0.0403
Cu	0.112	0.0325
Sn	n/a	n/a

Determining the size of the RT-modeled tin atom's electron on the fifth level:

$$r_{e5} = \frac{T_5 \cdot \alpha}{8\pi \cdot n} = \frac{88.8 \cdot 10^{-9}}{8\pi \cdot 137 \cdot 5} = 5.16 \cdot 10^{-12}\, m,$$

Sn (for 5s) $T = 88.8$ nm, then $r_{e5} = 25.81 \cdot 10^{-12}$ m .

4.4 ELECTRON LEVITATION

A quantum mechanically characterized model of matter utilizes the probabilistic approach to simulate the occurrence of the monitored object, proposing that a given particle is, with a probability $p\ (t, x, y, z)$ and at a time t, present at a location defined by the coordinates x, y, z of the Cartesian system. However, when comparing the experimentally measured distances and angles in atomic groupings of various elements, we find precise and always equal mean quantity values, such as those in Fig. 39. The dispersion of the instantaneous values of the quantities is not a critical parameter, with respect to the mean value of the given quantity. Due to these factors, the quantum mechanical model cannot be regarded as very suitable for explaining the formation of the interatomic bonds in, for example, regular structures and crystal lattices.
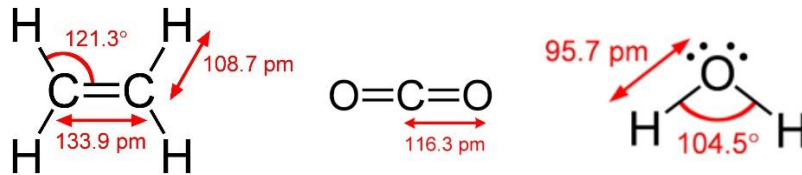

Fig. 38 The mean values of the distances and angles in groups of diverse elements combined into molecules.

Ring theory and the designed model of the structure of matter nevertheless enable us to determine markedly more easily (in an explicit manner) the place where the electron "occurs" at a given time (without the need of sophisticated and indefinite probabilistic functions expressed implicitly) because the electron, if modeled via RT, is maintained in position by a dynamic electromagnetic field; using an explicit description, we can then suggest that the axis of the modeled electron is identical with that of the ring of the proton, to which the electron couples in the atomic nucleus. The electron's levitation distance from the nucleus is determined by the balance between the attractive and the repulsive forces existing in the electromagnetic fields of the electron, proton, and neutron.

Coupled electric fields, namely, those of the negative electric charge q_e of the modeled electron and the positive charge q_p of the modeled proton, lead to mutual action of forces and dynamic balance between the particles, these being processes or states that embody counterbalance to the coupled magnetic fields of the particles with antiparallel spins (Fig. 40). Although the model of the neutron is assumed without the resulting external electric charge q_n, the positive and the negative electric charges of the quarks inside the neutron form a magnetic field that couples to the magnetic field of the proton; this field then acts on the electron through a joint electrodynamic force, especially in the neutron–proton–electron axis. The balance between these electric and magnetic forces ensures electrodynamic stability (levitation) of the electron, which is situated in a dynamically balanced position on the common axis.

In the RT-based model, the electron does not revolve around the atomic nucleus, and its position is not expressed implicitly; rather than this, the electron is located at a certain distance, with the parameters expressed explicitly, and it is confined to the structure of the nucleus by electromagnetic dynamic forces (Fig. 40).
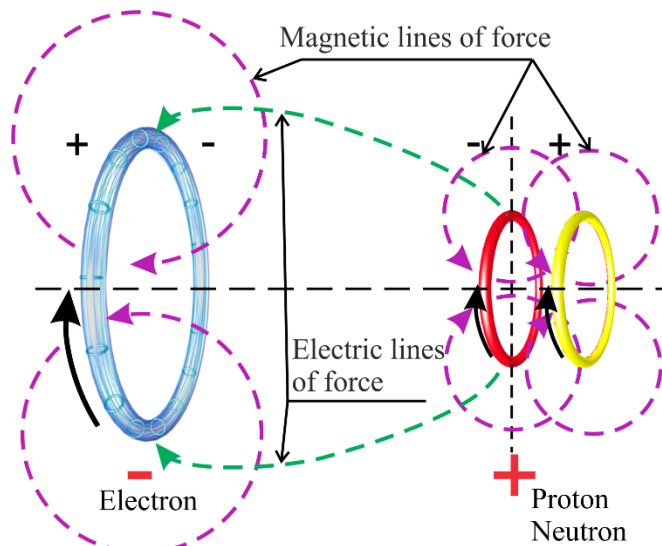
Fig. 39 An electron levitating in the RT-based model of the atom.

Let us assume, according to Fig. 41a), a ring-shaped proton whose center is situated at the origin o of the relevant local coordinate system, with the toroid having a radius r_p, and let us also assume a point P_e at a distance r', outside the axis of the toroid. The toroid carries a current of an instantaneous value i, and a fundamental current path $i\,ds$ can be defined on the toroid's length element ds. The angles between the origin of the toroid and the point P_e and between the current element $i\,ds$ and axis x are shown in Fig. 41a), denoted by θ and φ, respectively.

a)

b)   c)
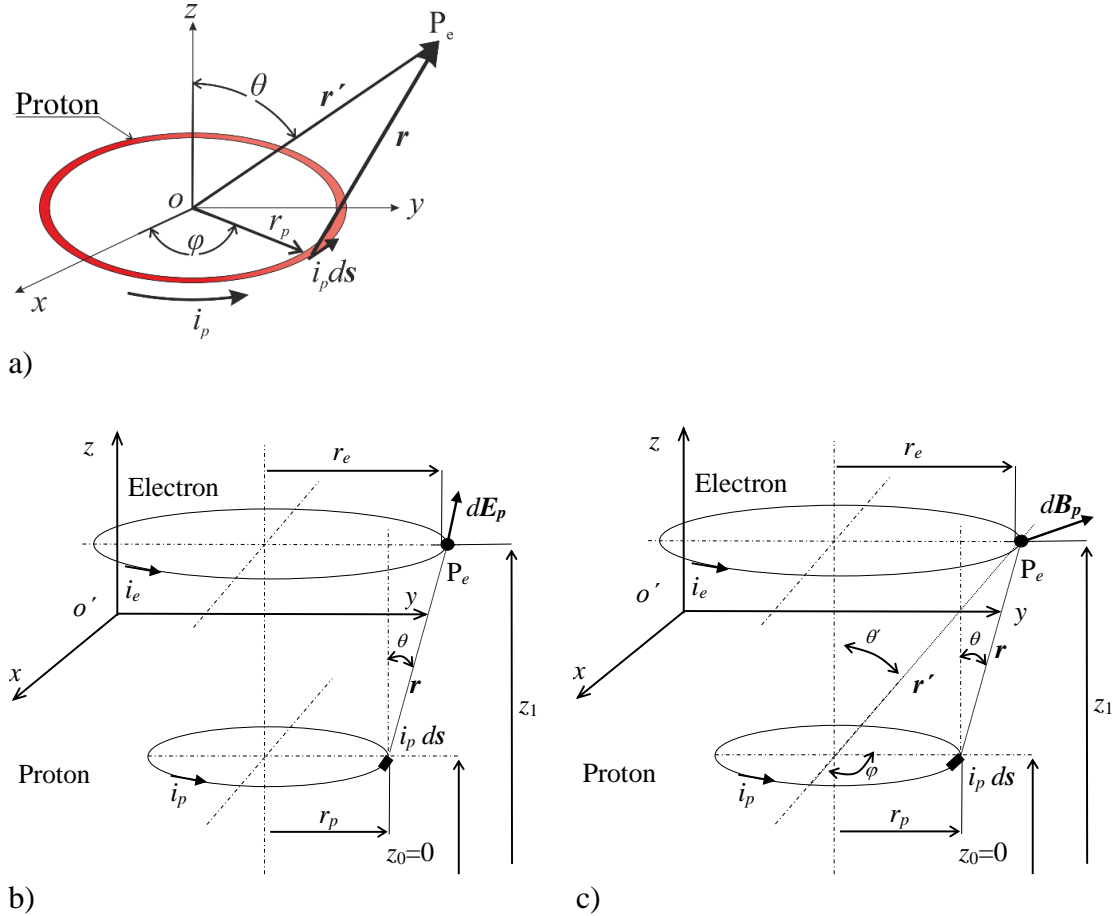
Fig. 40 The configuration of the elementary components in the proton ring, a); the proton–electron electric field, b); and c) the magnetic field outside the symmetry axis of the proton current loop (proton-electron).

25

The electric current having an instantaneous value to derive the relationships between the acting forces is assumed to be

$$i(t) = \frac{dq}{dt}, \qquad q_e = -q_p; \tag{15}$$

the current of the proton is then expressed as

$$i_p = \frac{dq_p}{dt}, \tag{16}$$

and that of the electron as

$$i_e = -\frac{dq_e}{dt}. \tag{17}$$

A simple application of the Biot-Savart law leads to an expression of the relationship between the increment of the specific magnetic flux $d\boldsymbol{B}_p$ and the length element $d\boldsymbol{s}$:

$$d\boldsymbol{B}_p = \frac{\mu_0}{4\pi} \frac{i_p \, d\boldsymbol{s} \times \boldsymbol{r}}{\|\boldsymbol{r}\|^3}. \tag{18}$$

When abbreviated, the contribution of the current element is written as

$$d\boldsymbol{\eta}_p = i_p \, d\boldsymbol{s}, \tag{19}$$

and the contribution of the magnetic field becomes

$$d\boldsymbol{B}_p = \frac{\mu_0}{4\pi} \frac{d\boldsymbol{\eta}_p \times \boldsymbol{r}}{\|\boldsymbol{r}\|^3}. \tag{20}$$

After further reduction, the formula defining the magnetic flux increment in the selected coordinate system will be available for simplified use.

It follows from the reduced equation (20) that the magnetic field generated by the proton and filling the space of the electron is oriented in the positive radial direction of the ring electron; in the other direction, the component's orientation is towards the ring proton. For an analysis of the dynamic relationship between the proton and the electron as regards the action of forces, the force increment amounts to

$$d\boldsymbol{F}_m = q_e \, \boldsymbol{v} \times d\boldsymbol{B}. \tag{21}$$

According to the above-presented RT model, the electron and the proton (neutron) exhibit diverse structures. In the proton, the magnetic field consists of three quarks and three gluons, whose electric charges move within the given toroidal space at a speed different from that of the charges of the electron; the corresponding magnetic fields are thus expected to vary, Figs. 7 to 9. Consequently, in an expression of the fields and forces, the assumed instantaneous value of the current i(t) related to the length element $d\boldsymbol{s}$ has to respect the fact that the excitation elements consist in the electric charges of the ring proton and electron, with the charge of the latter moving multiply more slowly; such a property then allows the charge to be interpreted as a point, P_e, in relation to the $id\boldsymbol{s}$ of the proton. This definition of the velocities of the electron's and the proton's electric charges is matched by the configurations of the magnetic field and the electric charge at P_e, as displayed in Fig. 41a) and Fig. 41b). The reduced and more accurately specified electron – proton dynamic relationship finds, through spherical coordinates applied to the Cartesian coordinate system, the following formal representation:

$$d = z_1 - z_0, \text{ for } z_0 = 0, \tag{22}$$

$$\boldsymbol{r} = r_p \cos\varphi \, \boldsymbol{u}_x + \left(r_e - r_p \sin\varphi\right)\boldsymbol{u}_y + d \, \boldsymbol{u}_z, \tag{23}$$

$$d\boldsymbol{\eta}_p = i_p \, r_p d\varphi_p \left(\cos\varphi \, \boldsymbol{u}_x + \sin\varphi \, \boldsymbol{u}_y\right), \tag{24}$$

Utilizing formula (18) for the selected coordinate system, we then have

$$d\,\boldsymbol{s}\times\boldsymbol{r}=\begin{vmatrix} \boldsymbol{u}_x & \boldsymbol{u}_y & \boldsymbol{u}_z \\ r_p cos\varphi d\varphi & r_p sin\varphi d\varphi & 0 \\ r_p cos\varphi & \left(r_e-r_p sin\varphi\right) & d \end{vmatrix},\tag{25}$$

$$d\,\boldsymbol{s}\times\boldsymbol{r}=\boldsymbol{u}_x\left(r_p d\,sin\varphi\,d\varphi\right)+\boldsymbol{u}_y\left(-r_p d\,cos\varphi\,d\varphi\right)+\boldsymbol{u}_z\left(r_p cos\varphi\,d\varphi\left(r_e-r_p\,sin\varphi\,d\varphi\right)-r_p cos\varphi\,r_p\,sin\varphi\,d\varphi\right),\tag{26}$$

$$d\,\boldsymbol{s}\times\boldsymbol{r}=\boldsymbol{u}_x\left(r_p d\,sin\varphi\,d\varphi\right)+\boldsymbol{u}_y\left(-r_p d\,cos\varphi\,d\varphi\right)+\boldsymbol{u}_z\left(r_p r_e\,cos\varphi\,d\varphi-2r_p^2 cos\varphi sin\varphi\,d\varphi\right),$$

and the magnetic flux density contribution is expressed as

$$d\,\boldsymbol{B}_p=\frac{\mu_0}{4\pi}i_p\frac{\boldsymbol{u}_x\left(r_p d\,sin\varphi\,d\varphi\right)+\boldsymbol{u}_y\left(-r_p d\,cos\varphi\,d\varphi\right)+\boldsymbol{u}_z\left(r_p r_e\,cos\varphi\,d\varphi-2r_p^2 cos\varphi sin\varphi\,d\varphi\right)}{\left(r_p^2 cos^2\varphi+\left(r_e-r_p sin\varphi\right)^2+d^2\right)^{\frac{3}{2}}}.\tag{27}$$

After reduction, we can write

$$\boldsymbol{B}_p=\frac{\mu_0}{4\pi}r_p i_p\left(\int_0^{2\pi}\frac{\boldsymbol{u}_x\left(d\,sin\varphi\right)+\boldsymbol{u}_y\left(-d\,cos\varphi\right)+\boldsymbol{u}_z\left(r_p r_e\,cos\varphi\,d\varphi-2r_p^2 cos\varphi sin\varphi\,d\varphi\right)}{\left(r_p^2 cos^2\varphi+\left(r_e-r_p sin\varphi\right)^2+d^2\right)^{\frac{3}{2}}}d\varphi\right),\tag{28}$$

$$\Delta\boldsymbol{F}=-i_e d\boldsymbol{\ell}\times d\,\boldsymbol{B},\tag{29}$$

$$\Delta\boldsymbol{F}=-i_e\begin{vmatrix} \boldsymbol{u}_x & \boldsymbol{u}_y & \boldsymbol{u}_z \\ r_e d\varphi & 0 & 0 \\ B_x & B_y & B_z \end{vmatrix}.\tag{30}$$

For the evaluated component of force at a single point P, such component being independent of the coordinate φ, we then have

$$\Delta\boldsymbol{F}=-i_e\left(-B_z r_e d\varphi\,\boldsymbol{u}_y+B_y r_e d\varphi\,\boldsymbol{u}_z\right),\tag{31}$$

and formulas (26-28) will yield the force components acting at the point P, such components depending on the coordinate φ, as

$$\Delta\boldsymbol{F}=-i_e\begin{vmatrix} \boldsymbol{u}_x & \boldsymbol{u}_y & \boldsymbol{u}_z \\ r_e sin\varphi d\varphi & r_e cos\varphi d\varphi & 0 \\ dB_x & dB_y & dB_z \end{vmatrix}\tag{32}$$

$$\Delta\boldsymbol{F}=-i_e\left(dB_z r_e cos\varphi d\varphi\,\boldsymbol{u}_x-dB_z r_e sin\varphi d\varphi\,\boldsymbol{u}_y+\left(dB_y r_e sin\varphi d\varphi-dB_x r_e cos\varphi d\varphi\right)\boldsymbol{u}_z\right).\tag{33}$$

Assuming the contribution of the forces to the fixed point P according to equation (31), the force component takes the form

$$\Delta\boldsymbol{F}=\frac{\mu_0}{4\pi}r_e r_p i_p i_e\left(\left(\int_0^{2\pi}\frac{\left(r_e cos\varphi-2r_p cos\varphi sin\varphi\right)}{\left(r_p^2 cos^2\varphi+\left(r_e-r_p sin\varphi\right)^2+d^2\right)^{\frac{3}{2}}}d\varphi\right)\boldsymbol{u}_y\right.$$

$$\left.+\left(\int_0^{2\pi}\frac{d\,cos\varphi}{\left(r_p^2 cos^2\varphi+\left(r_e-r_p sin\varphi\right)^2+d^2\right)^{\frac{3}{2}}}d\varphi\right)\boldsymbol{u}_z\right),\tag{34}$$

27

and for the case of dependence on the coordinate φ, shown in formula (32), we have

$$\Delta \boldsymbol{F} = -\frac{\mu_0}{4\pi} r_e r_p i_p i_e \left(\left(\left(\int_0^{2\pi} \frac{r_e \cos^2\varphi - 2r_p \cos^2\varphi \sin\varphi}{\left(r_p^2 \cos^2\varphi + \left(r_e - r_p \sin\varphi \right)^2 + d^2 \right)^{\frac{3}{2}}} d\varphi \right) \boldsymbol{u}_x \right. \right.$$

$$- \left(\int_0^{2\pi} \frac{r_e \cos\varphi \sin\varphi - 2r_p \cos\varphi \sin^2\varphi}{\left(r_p^2 \cos^2\varphi + \left(r_e - r_p \sin\varphi \right)^2 + d^2 \right)^{\frac{3}{2}}} d\varphi \right) \boldsymbol{u}_y \right)$$

$$\left. \left. - \left(\int_0^{2\pi} \frac{2d \cos\varphi \sin\varphi}{\left(r_p^2 \cos^2\varphi + \left(r_e - r_p \sin\varphi \right)^2 + d^2 \right)^{\frac{3}{2}}} d\varphi \right) \boldsymbol{u}_z \right) \right) \quad . \tag{35}$$

Evaluating the force ΔF leads to a relationship with elliptic integrals and rather complex expressions.

The resulting magnetic force F acting towards the axes of the rings of the modeled atom H between the proton and the electron will be considered in the entire model, as indicated in formula (35), respecting the assumed sizes of the proton and electron rings and the velocity of the electric charge q propagating along the perimeters of both modeled elements. In the above formulas, i_e is the electric current generated by a moving electric charge q_e in the electron; r_e denotes the radius of the electron; i_p represents the electric current created by the moving electric charge in the proton, q_p; r_p stands for the radius of the proton; and d is the distance between the proton and the electron on their common axis (Fig. 41c).

Next, to define the action of the electric force $\boldsymbol{F}_e$ (Fig. 41b), Fig. 42), we determine the distance according to formula (23); the initial view of the intensity increment, Fig. 41b), is then expressed as

$$d\boldsymbol{E} = \frac{dq}{4\pi\varepsilon_0 \, r^2} \cos\theta \, \boldsymbol{u}_z \quad . \tag{36}$$

To facilitate integration around the perimeter of the proton, the contribution of the electric field intensity (Fig. 42) is expressed as

$$d\boldsymbol{E} = \frac{dq \left(r_p \cos\varphi \, \boldsymbol{u}_x + \left(r_e - r_p \sin\varphi \right) \boldsymbol{u}_y + d \, \boldsymbol{u}_z \right)}{4\pi\varepsilon_0 \left(r_p^2 \cos^2\varphi + \left(r_e - r_p \sin\varphi \right)^2 + d^2 \right)^{\frac{3}{2}}} \quad . \tag{37}$$

The electric field intensity for the linear distribution and density of the electric charge τ is then embodied in the formula

$$\boldsymbol{E} = \int_0^{2\pi} d\boldsymbol{E} \, , \tag{38}$$

$$\boldsymbol{E} = \int_0^{2\pi} \tau r_p \frac{\left(r_p \cos\varphi \, \boldsymbol{u}_x + \left(r_e - r_p \sin\varphi \right) \boldsymbol{u}_y + d \, \boldsymbol{u}_z \right)}{4\pi\varepsilon_0 \left(r_p^2 \cos^2\varphi + \left(r_e - r_p \sin\varphi \right)^2 + d^2 \right)^{\frac{3}{2}}} d\varphi \, . \tag{39}$$

The contribution of the electric force acting on the electric charge q_e in the axis at the distance d is

$$d\boldsymbol{F}_{el} = q_e \cdot d\boldsymbol{E} \, , \tag{40}$$

and, regarding the component of the force $\Delta \boldsymbol{F}_e$ at the single point P independent of the coordinate φ, we then have

28

$$\Delta \boldsymbol{F}_{el} = q_e \cdot \int_{\varphi} d\boldsymbol{E} \tag{41}$$

$$\Delta \boldsymbol{F}_{el} = \frac{q_e q_p}{4\pi\varepsilon_0} \int_0^{2\pi} \frac{\left(r_p cos\varphi\, \boldsymbol{u}_x + \left(r_e - r_p sin\varphi\right)\boldsymbol{u}_y + d\,\boldsymbol{u}_z\right)}{\left(r_p^2 cos^2\varphi + \left(r_e - r_p sin\varphi\right)^2 + d^2\right)^{\frac{3}{2}}} d\varphi \, . \tag{42}$$
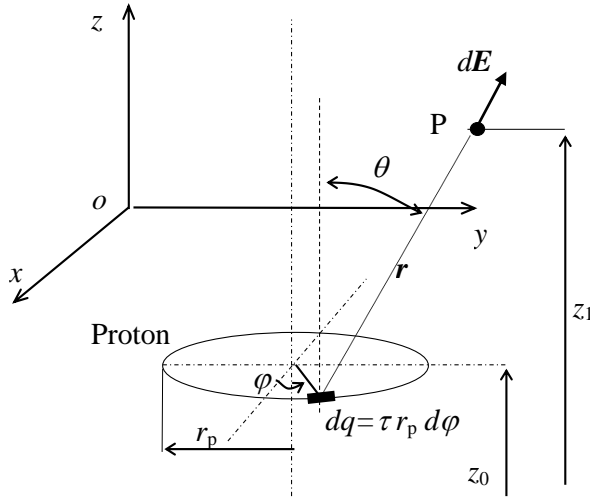
Fig. 41 Determining the electric field intensity at the point P outside the axis of the ring.

In the dynamic balanced state, namely, levitation of the modeled electron, the magnitudes of the electric and magnetic forces are in balance but act on each other in an opposite direction, assuming the given configuration; we can then write

$$\left\|\boldsymbol{F}_{el}\right\| = \left\|\boldsymbol{F}_{mg}\right\|, \ \left|\boldsymbol{F}_{el}\right| = -\left|\boldsymbol{F}_{mg}\right| \ . \tag{43}$$

5 MODELING THE ATOM VIA RT

The proposed deterministic structural concept of the atomic nucleus interpreted from the perspective of the electromagnetic field enables us to explicitly localize and express the positions of the individual elements of the atom, even in atoms having a very complex structure of the nucleus. The position, location, and parametric description of the modeled electrons in the shells are, however, determined by not only the axes of the corresponding protons but also other factors, including the action of forces produced by electrons in neighboring shells, nuclear components, and inter-proton magnetism.

In the electron and the proton, the dynamic balanced state at the individual energy levels requires as a necessary precondition the presence of opposite spins (magnetic moments) and relevant negatively acting forces of the magnetic field on the electron-proton axis. The neutron, if neighboring in the globule on the proton, contributes to the overall intensity of the proton's magnetic field, thus also contributing to the oppositely oriented vector of forces and generating the repulsive force of the proton's magnetic field with respect to the electron on the common axis. In this context, a significant effect consists in the nonlinear growth of the electron's magnetic field when the particle occupies the higher energy levels. The balanced state of the dynamic forces developed by electrons at the atomic energy levels results from, among other aspects, a marked influence of the repulsive force generated by the magnetic field existing between the electron, the proton, and its two neighboring neutrons in the nucleus on the forces of the electric field with charges q; no shielding impact of the other electrons manifests itself in the analyzed situation.

In hydrogen, the simplest of the modeled chemical elements, the nucleus consists of a single proton, and the shell comprises a single electron (Fig. 43), which does not revolve around the proton but remains in dynamic balance on the common axis at the quantifiable distance of $2.34 \cdot 10^{-11}$ m. If this (ring) electron is excited to an n-th higher energy level, it will move away from the proton on the common axis to an n-times greater distance, remaining in dynamic balance.
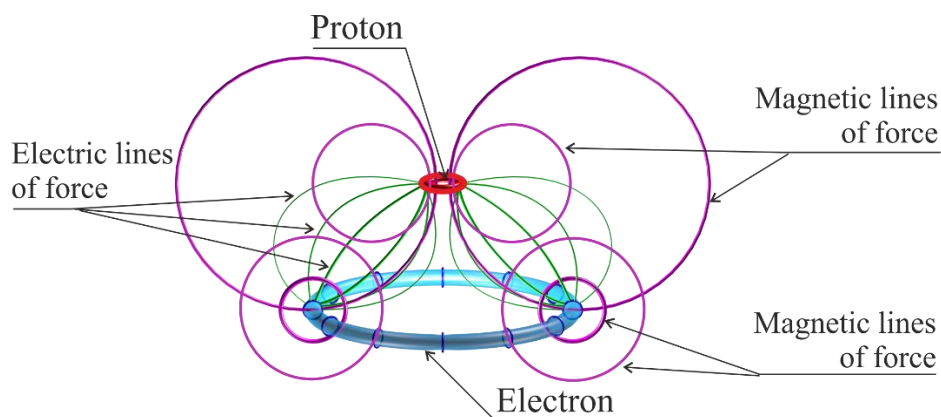
Fig. 42 The structure of the hydrogen atom, and the schematically represented electromagnetic fields.

As regards the isotopes of hydrogen (Fig. 44), the model of deuterium differs from that of hydrogen as a whole only moderately, containing one additional element: the neutron. The particle will cause, by gross approximation, a twofold increase in the intensity of the magnetic field H to maintain the balanced dynamic state; such a process will change the positions of the electron and proton rings to the quantifiable distance of $4.25 \cdot 10^{-11}$ m.

In tritium, the nucleus already contains one proton and two neutrons, whose own magnetic fields will move the electron ring to the distance of $5.5 \cdot 10^{-11}$ m (Eq. (84)), setting the system to the balanced dynamic state. Within the configuration, the attractive electrostatic forces are apparently

considerably weakened in comparison to those of the entire hydrogen, and thus, from the perspective of the balanced dynamic state, the isotope is unstable.
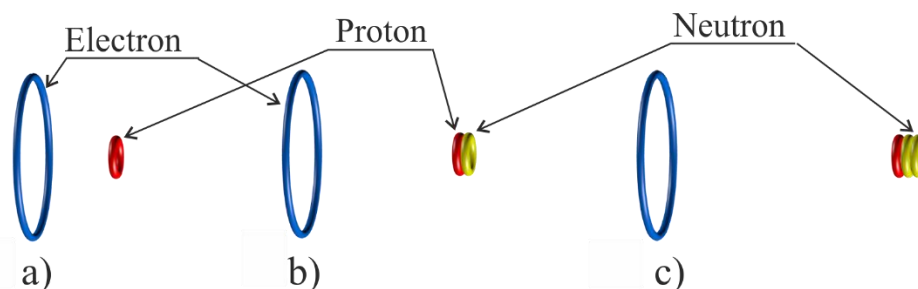

Fig. 43 A modeled chemical element and its isotopes: a) hydrogen; b) deuterium; and c) tritium.

It was shown in the above discussion that each of the modeled elementary particles is characterized by having merely a single spin instead of two, a "positive" and a "negative" one, as could be assumed from other hypotheses and models. In ring theory, the spin and its attributes are evaluated with respect to another particle, allowing us to determine whether the spin's orientation is parallel, namely, the vectors point in the same direction, or antiparallel, with the spin vectors directed oppositely. This procedure and capability embody major parameters for specifying electron - nucleus couplings and also bonds between the atoms and molecules of the structures and substructures.

The modeled hydrogen atom may exist in two equal states where the spins are positioned in an antiparallel manner (Fig. 45).
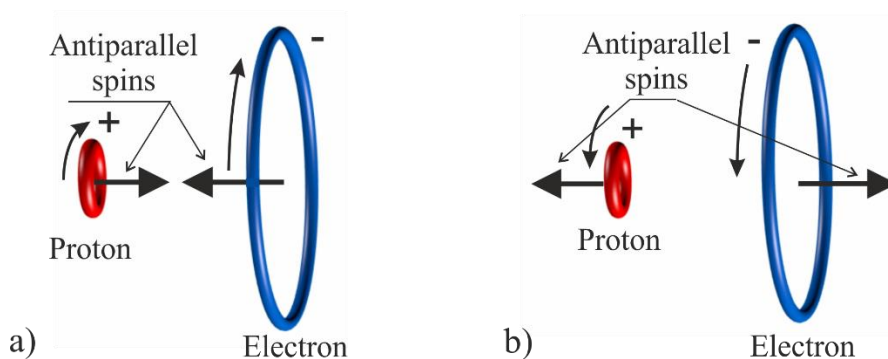
Fig. 44 The two opposite states of hydrogen atoms with antiparallel spins.

These states, taken to be a description parameter for the model, are indispensable for classifying the nuclear globules' coupling relationships and evaluating the action of forces in the differerent spin types; the character of the proton and neutron spins always varies between neighboring globules.

If stand-alone proton and electron rings having parallel spins act on each other through their electric and magnetic fields, the resulting force will be attractive and greater than that accompanying the scenario with antiparallel spins, in which the magnitude of the force follows from the difference between the corresponding magnetic field strengths, Fig. 46a. The modeled proton and electron will adjust their geometries to lie in a common plane determined by the plane of their rings (Fig. 47), with the proton in the middle. Regarding the arrangement comprising parallel spins, however, the electric charges of the proton and the electron rotate in opposite directions, against each other (Fig. 47); such an effect then leads to altered distribution of the electric and magnetic lines of force, a change which lowers the rotation velocities of the proton's and the electron's electric charges. The dynamic model of the electron responds to these events via progressive reduction of the radius and simultaneous energy emission. During the reduction of the radius and energy to the basic values (11), the charges

moving in opposite directions and at various velocities v will induce positional instability in the proton ring, shifting it outside the relevant plane until the electron flips over above the plane perpendicular to that of the proton, with the particles' spins positioned against each other in an antiparallel manner (Fig. 47).
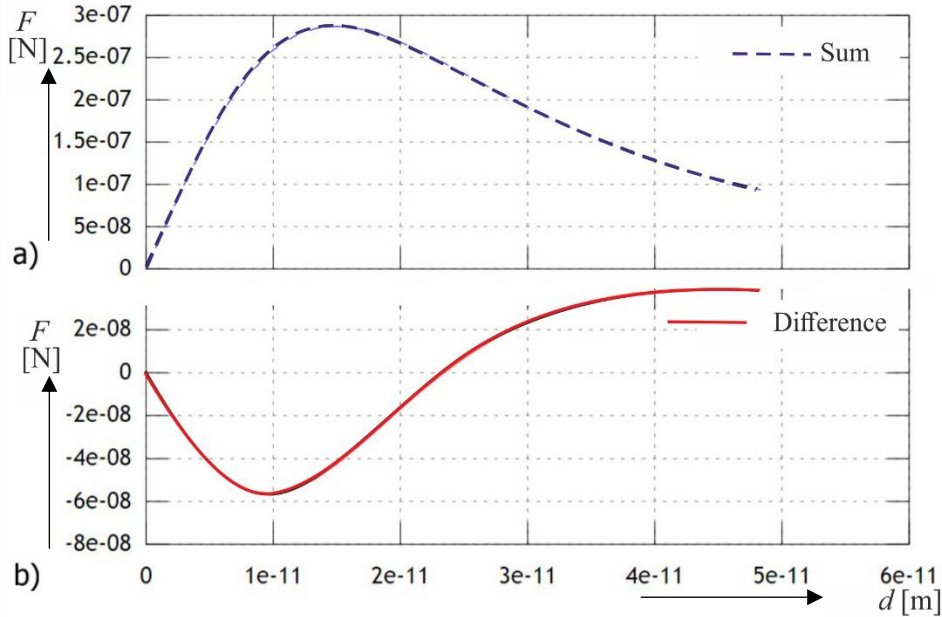

Fig. 45 The orientation and magnitudes of the forces in the axis of the rings, related to a) parallel and b) antiparallel spins of the hydrogen atom.
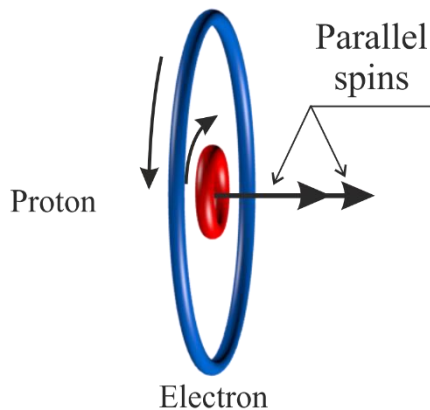

Fig. 47 The hydrogen atom with parallel spins of the proton and the electron.

The modeled helium atom, Fig. 48, has a nucleus containing two protons and two neutrons. This configuration then embodies the simplest (and a unique) concept or structure of the globule, termed "alpha particle"; the structure is held together by electrodynamic forces generated by the electromagnetic fields of the toroids.
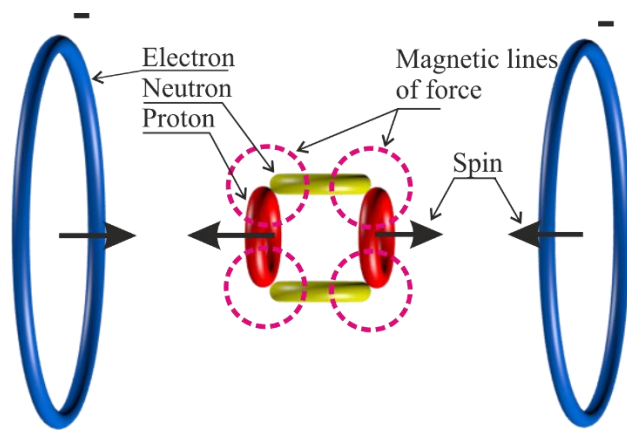
Fig. 46 The modeled helium atom.

In the modeled atoms, the electron shell, geometries, parameters, and other aspects are determined by the designed atomic nucleus structure. According to RT and the associated structural model, electrons do not revolve around the nucleus in circular orbits, as proposed by previous theories, but the path of the future electric charge q_e of the toroidal electron remains on the coordinate that, within the configuration of the nucleus, expresses the balanced dynamic state (Fig. 48).

The magnetic forces undergo step changes at the individual energy levels, where they are further differentiated by the quantum number "l". The nuclear electric force acting on the electron grows with increasing proton number; here, however, we have to consider the limitation posed by the amount of protons in the globule and its vicinity, to which the electron is bound. The electric forces inside the atom predetermine the effects arising from the arrangement of the globules, which are separated from one another and maintained in their positions by the balance of the dynamic forces, otherwise also referred to as the proton bridge.

As the atomic number a rises, the electrons at the lower energy levels become increasingly more attracted to the nucleus, reducing their radii r_e, the radius of the energy orbital level, and, consequently, also the radius of the entire modeled atom (Fig. 49).
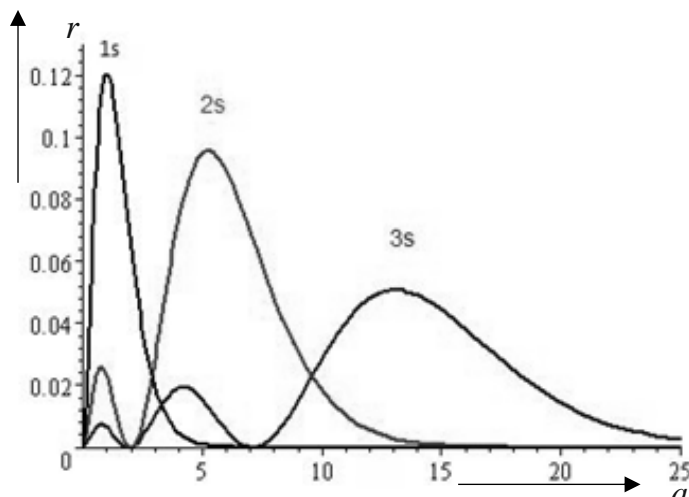
Fig. 47 The electron radii at the lower energy levels change with the increasing atomic number "a".
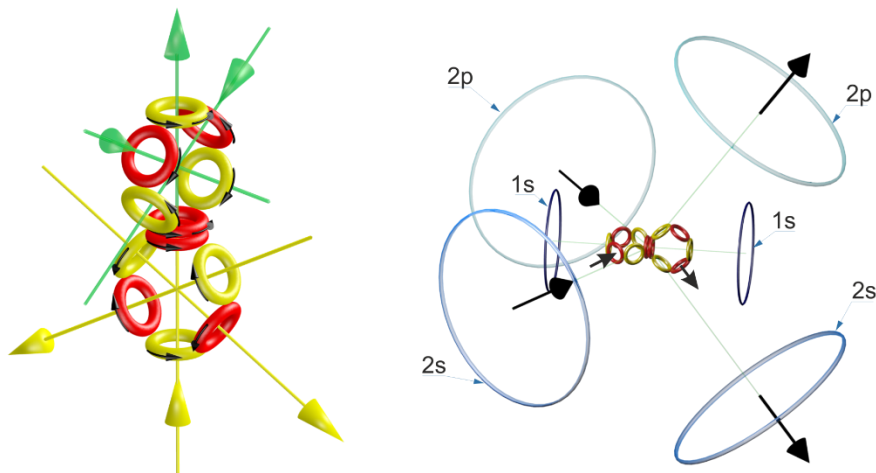
Fig. 48 The directions, orientation, and distribution of the electron spins in the modeled carbon atom nucleus.

The structure of the atomic nucleus together with the distribution of the electrons, spins, and electromagnetic fields facilitate explanation of the structure of the electron shell of the atom and also various interatomic and intermolecular bonds, Figs. 50 and 51.
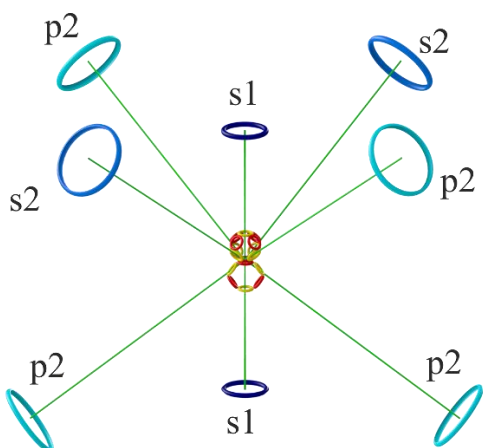
Fig. 49 The distribution of electrons in the oxygen atom.

The modeled distribution of the electrons occupying the energy levels 3p and 3d enables us to explain easily the magnetic properties of the iron atom, Fig. 52.
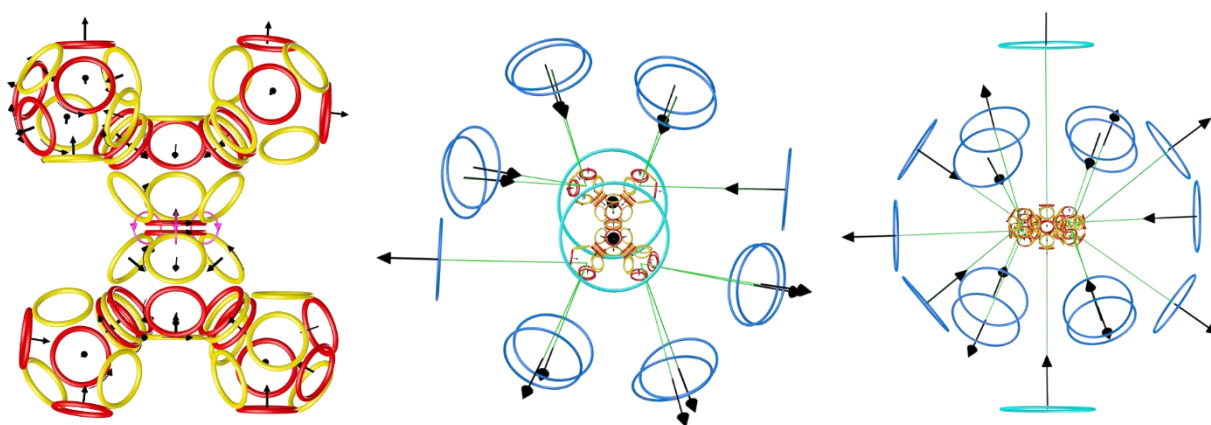
Fig. 50 The setup and orientation of the spins in the iron atom nucleus. Illustrative views: a) front; b) side.

34

5.1 EXPRESSING AND QUANTIFYING THE FORCES AND DISTANCES IN THE MODELED ATOMS

In the structure of matter as interpreted through RT, the geometrical arrangement of the electron is electromagnetically influenced by the proton located on the common axis. The toroids become dynamically balanced, and the forces of the electric and the magnetic components of the field are in equilibrium. These forces then cause the proton and the electron to approach each other in the axis perpendicular to their rings; simultaneously, the forces' components in the axis of the relevant ring bring about reduction of the radius of the electron, R_1. The internal electromagnetic forces of the electron's substructures respond to the change up to a certain limit; at this boundary, the toroid's structure rapidly changes (Figs. 1, 53, and 54), its radius R_1 decreases by a half-wave ($\lambda/2$), the magnetic field is made smaller, and energy in the form of a photon is released. After the geometry of the electron has shrunk to the baseline state of one half-wave ($\lambda_1/2$) and the proton has been approached to the distance that equals the radius of the electron (R_1), the magnetic force in the plane of the ring will transform from attractive to repulsive. This force, combined with that of the electric field, will subsequently produce a balanced condition, Fig. 53. The internal electrodynamic forces of the electron are thus in equilibrium with the external forces exerted by the proton, leading to a stable balanced state.

The ring of the electron (Fig. 53) is subjected to a magnetic force from the inhomogeneous magnetic field of the proton; the axis of the proton ring, however, experiences only a very minimal magnetic impact, as the corresponding field of the electron (considering the toroid's size) is distributed markedly homogeneously at the location of the proton.
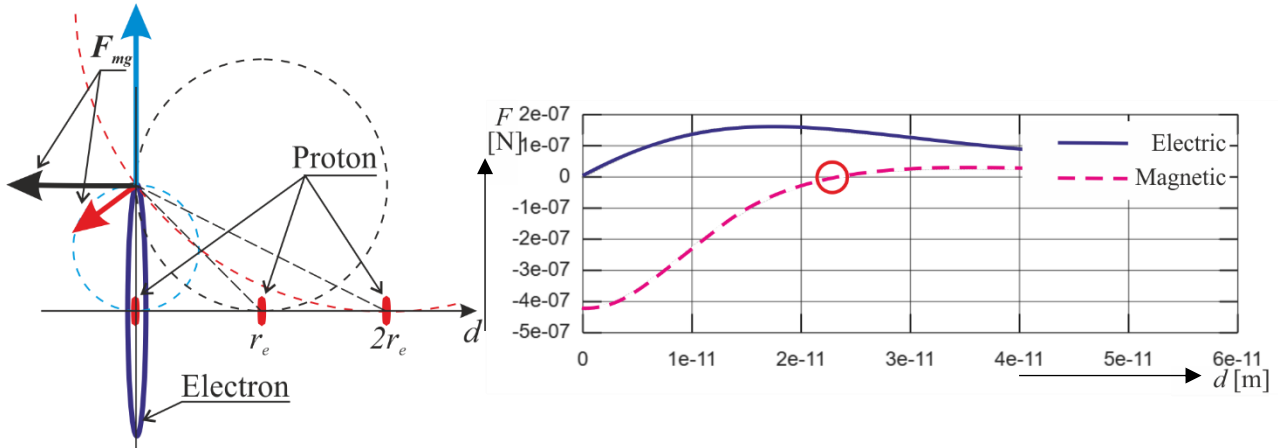
Fig. 51 The altered orientation of the magnetic force acting in the axis y if the distance is shorter than the radius of the electron, R_1.

5.2 MODEL OF THE HYDROGEN ATOM

The fundamental concept to quantify the explicit model of the H atom and to specify the levitation distances rests in balanced electric and magnetic forces between the models, namely, the comparatively large ring of the electron and the substantially smaller toroidal proton. For the dimensions in the hydrogen atom, let us assume

$$r_p \ll r_e , \ r_p \ll d ; \tag{44}$$

as regards the force vector components, we then have
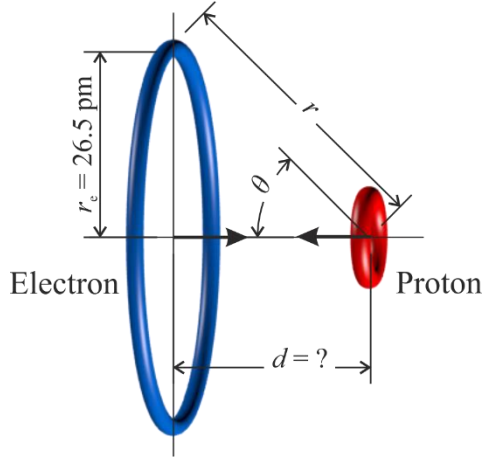
$$F_{el,z} = F_{mg,z} . \tag{45}$$

Fig. 52 The modeled hydrogen atom.

Using Coulomb's law to calculate the electrostatic force between the proton and the electron in Bohr's model of the hydrogen atom will yield for the distance $d = 0$ an infinite value of force (Figs. 55 and 56), the appropriate formula being

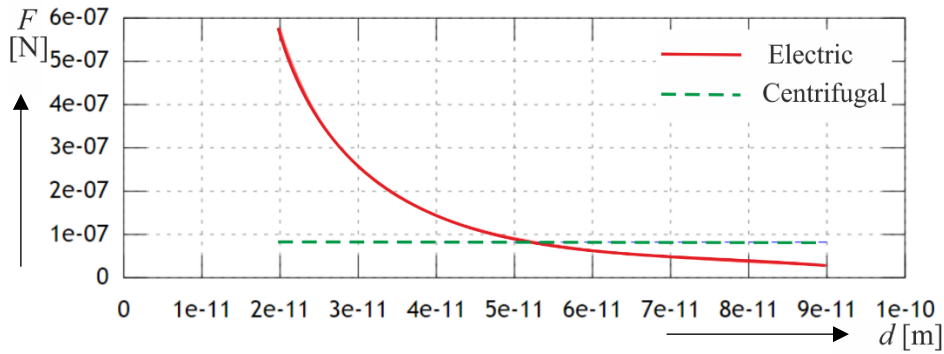$$F_{el-p} = -\frac{q_e q_p}{4\pi\varepsilon_o}\left(\frac{1}{r^2}\right).$$

(46)

Fig. 53 The electrostatic and centrifugal forces in Bohr's model of the hydrogen atom.

But if the electrostatic force between the proton and the electron is analyzed and evaluated according to the RT-based solution comprised in Eq. (42), we will obtain a different value: Considering the distance $d = 0$, the magnitude of the module of the electrostatic force F_{el} in the hydrogen atom model will equal $F_{el} = 0$ (Fig. 56). We have

$$F_{el-p,z} = -\frac{q_e q_p}{4\pi\varepsilon_o}\frac{\cos\theta}{r^2},$$

(47)

$$F_{el-p,z} = \frac{q_e q_p}{4\pi\varepsilon_o}\frac{d}{\sqrt{(d^2 + r_e^2)^3}},$$

(48)

where d denotes the distance between the proton and the electron in the axis of their rings, and r_e is the diameter of the modeled electron.
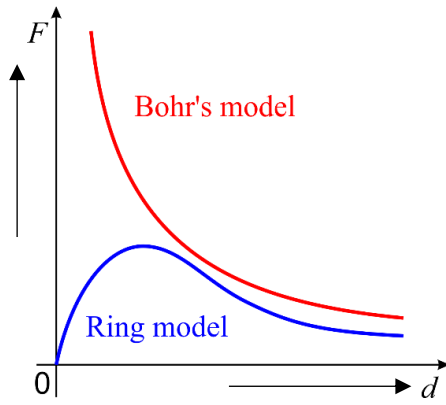
Fig. 54 The electrostatic force module: the Bohr and the ring models of the hydrogen atom compared.

The magnitude of the magnetic field of the proton at the point P on the electron ring is determined by applying the Biot-Savart law, as shown within formulas (21) - (34); subsequently, we will be able to evaluate the corresponding magnetic force in the axis z.
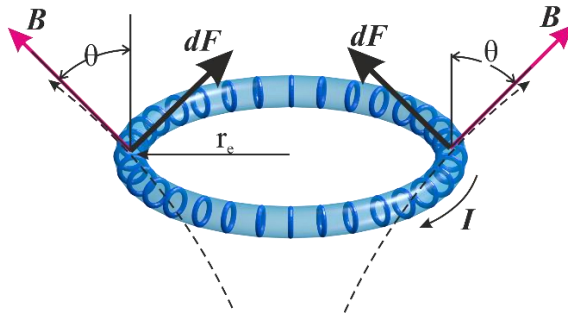
Fig. 55 The interaction of the proton's magnetic field and the electron.

The magnetic force acting in the direction of the axis z, between the proton and the electron rings in the hydrogen atom, will be assumed based on the above-derived Eqs. (21) and (34), by means of the magnetic moments of the proton and the electron:

$$\mu_p = i_p \cdot \pi r_p^2, \ \mu_e = i_e \cdot \pi r_e^2 . \tag{49}$$

The expression can be simplified in the spherical coordinate system to become

$$d\,\boldsymbol{B}_p = \frac{\mu_0}{4\pi} \frac{d\boldsymbol{\eta}_p \times \boldsymbol{r}}{\|\boldsymbol{r}\|^3} \ , \tag{50}$$

$$d\,\boldsymbol{s} \times \boldsymbol{r} = \begin{vmatrix} \boldsymbol{u}_r & \boldsymbol{u}_\theta & \boldsymbol{u}_\varphi \\ 0 & 0 & r_p d\varphi \\ -r_p sin\theta & -r_p cos\theta & -r_p \end{vmatrix}, \tag{51}$$

$$\boldsymbol{B}_p = \frac{\mu_0}{4\pi} i_p r_p \left(\frac{\int_0^{2\pi} -\boldsymbol{u}_r \left(-r_p cos\theta d\varphi \right) + \int_0^{2\pi} \boldsymbol{u}_\theta \left(-r_p sin\theta d\varphi \right)}{\|\boldsymbol{r}\|^3} \right) . \tag{52}$$

After referring to formula (44), we will, for the given case, specify the magnetic flux density at the point P as

$$\boldsymbol{B}_p \cong \frac{\mu_0}{4\pi \|\boldsymbol{r}\|^3} i_p r_p \left(r_p cos\theta \int_0^{2\pi} \boldsymbol{u}_r \, d\varphi - r_p sin\theta \int_0^{2\pi} \boldsymbol{u}_\theta \, d\varphi \right), \tag{53}$$

37

$$B_p \cong \frac{\mu_0}{4\pi \|r\|^3} \mu_p cos\theta\, u_r - \frac{\mu_0}{4\pi \|r\|^3} \mu_p sin\theta\, u_\theta, \tag{54}$$

$$\Delta F = -i_e d\ell \times d\, B, \tag{55}$$

$$\Delta F = -i_e \begin{vmatrix} u_r & u_\theta & u_\varphi \\ 0 & 0 & r\, sin\theta d\varphi \\ B_r & B_\theta & 0 \end{vmatrix}. \tag{56}$$

Then, for the component of force at the single point P, independent of the coordinate φ, we have

$$\Delta F_P = -i_e \left(-B_\theta\, r\, sin\theta d\varphi\, u_r + B_r r\, sin\theta d\varphi\, u_\theta \right). \tag{57}$$

After reduction and simplification, the magnetic force at the point P, $F_{mg,z}$, can be written to yield

$$\Delta F_{mg} \cong i_e r\, d\varphi \frac{\mu_0}{4\pi \|r\|^3} \mu_p cos\theta sin\theta\, u_r - i_e rd\varphi \frac{\mu_0}{4\pi \|r\|^3} \mu_p sin^2\theta\, u_\theta, \tag{58}$$

$$\Delta F_{mg} \cong i_e \mu_p \frac{\mu_0}{4\pi \left(\sqrt{d^2 + r_e^2} \right)^3} r\, d\varphi sin\theta \left(cos\theta\, u_r - sin\theta\, u_\theta \right), \tag{59}$$

as schematically indicated in Fig. 58, and the simplified module of the force acting on the entire object (the modeled electron) is expressed in the form

$$F_{mg} \cong i_e \mu_p \frac{\mu_0}{4\pi \left(\sqrt{d^2 + r_e^2} \right)^3} \int_0^{2\pi} r\, sin\theta d\varphi.$$

Subsequently, however, considering the spot action on a part of the electron's space, namely, the point P, we have

$$F_{mg,P} \cong i_e \mu_p \frac{\mu_0}{4\pi \left(\sqrt{d^2 + r_e^2} \right)^3}; \tag{60}$$

involving only the component in the axis z will give

$$F_{mg,P,z} = \frac{i_e \mu_0 \mu_p sin2\theta}{4\pi \left(\sqrt{d^2 + r_e^2} \right)^3},$$

$$F_{mg,P,z} = \frac{i_e \mu_0 \mu_p 2dr_e}{4\pi \left(\sqrt{d^2 + r_e^2} \right)^5}, \tag{61}$$

where i_e denotes the current through the electron, r_e is the electron's radius, μ_p represents the magnetic moment of the proton, and d stands for the distance between the proton and the electron on their common axis (Fig. 58).
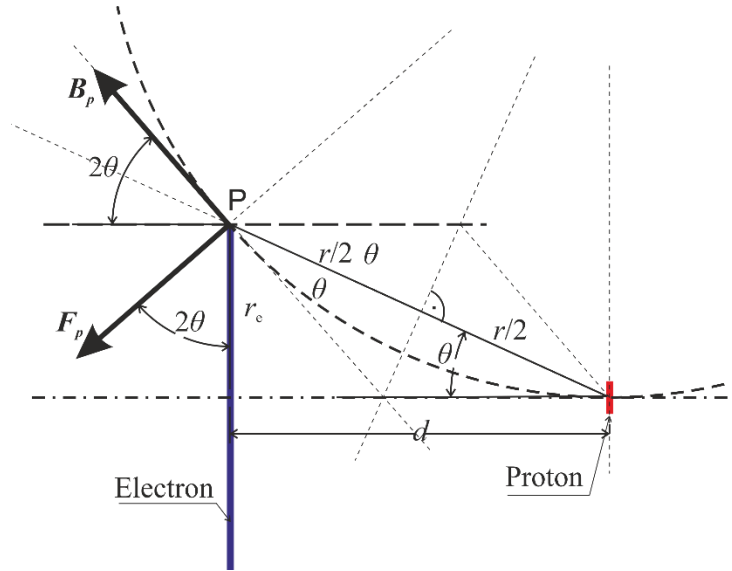
Fig. 56 The quantities in the hydrogen atom model to calculate the magnetic force F_P between the proton and the electron.

The radius r_e of the basic model of the hydrogen atom electron is established via the formula derived from the hydrogen atom spectrum (6):

$$r_e = \frac{T_1 \cdot \alpha}{8\pi \cdot n} = \frac{91.2324 \cdot 10^{-9}}{8\pi \cdot 137} = 26.5099 \cdot 10^{-12}\, m \,. \tag{62}$$

The time a photon requires to transfer its energy to the electron is longer by the value of the constant α than the time needed for the photon to travel the distance of its wavelength at the speed of light:

$$t_e = \frac{T_1}{c \cdot \alpha} = \frac{91.1 \cdot 10^{-9} \cdot 137}{3 \cdot 10^8} = 4.16 \cdot 10^{-14}\, s \,. \tag{63}$$

The current through the electron, i_e, which arises from the rotation of the electric charge q_e along the perimeter of the electron, or, more concretely, from one such cycle, is calculated via

$$i_e = \frac{q_e}{t_e} = \frac{1.602 \cdot 10^{-19}}{4.16 \cdot 10^{-14}} = 3.851 \cdot 10^{-6}\, A \,. \tag{64}$$

The charges and the magnetic fields of the proton and the electron act on each other at the distance of the hypotenuse r:

$$r = \sqrt{r_e^2 + d^2} \tag{65}$$

To obtain the attractive electric force in the axis z, $F_{el,z}$, we apply Coulomb's law:

$$F_{el,z} = \frac{1}{4\pi\varepsilon_0} \cdot \frac{q_e^2}{r^2} \cdot \cos\theta \,. \tag{66}$$

The magnetic force $F_{mg,z}$ in the axis x is expressed by means of the formula relating to the above-indicated closed toroid (Fig. 57) carrying the current i_e; at the location of the toroid, the magnetic flux density B makes the angle of 2θ with the normal, Fig. 58. The module of the proton's magnetic force acting on the small fundamental section of the electron ring ds that carries the current i_e is defined within Eq. (61), after whose reduction we have

$$F_{mg,z} = \frac{i_e \cdot \mu_0 \cdot \mu_p \cdot \sin 2\theta}{4\pi \cdot r^3} \,. \tag{67}$$

In the hydrogen atom, the levitation distance separating the proton from the electron at the basic energy level is given by the balance between the attractive electric and the repulsive magnetic forces:

39

$$F_{el,z} = F_{mg,z}, \tag{68}$$

$$\frac{1}{4\pi\varepsilon_0} \cdot \frac{q_e^2}{r^2} \cdot \cos\theta = \frac{i_e \cdot \mu_0 \cdot \mu_p \cdot \sin 2\theta}{4\pi \cdot r^3}, \tag{69}$$

$$\frac{1}{4\pi\varepsilon_0} \cdot \frac{q_e^2 \cdot d}{\sqrt{(r_e^2 + d^2)^3}} = \frac{i_e \cdot \mu_0 \cdot \mu_p \cdot 2 \cdot r_e \cdot d}{4\pi \cdot \sqrt{(r_e^2 + d^2)^5}}. \tag{70}$$

These formulas allow us to express the levitation distance d_l, yielding

$$d_l^2 = \frac{i_e \cdot \mu_0 \cdot \mu_p \cdot \varepsilon_0 \cdot 2 \cdot r_e}{q_e^2} - r_e^2, \tag{71}$$

$$d_l = \left(\frac{3.85 \cdot 10^{-6} \cdot 4\pi \cdot 10^{-7} \cdot 1.41 \cdot 10^{-26} \cdot 8.854 \cdot 10^{-12} \cdot 2 \cdot 2.65 \cdot 10^{-11}}{\left(1.6 \cdot 10^{-19}\right)^2} - \left(2.65 \cdot 10^{-11}\right)^2 \right)^{\frac{1}{2}}. \tag{72}$$

Substituting the known constants and calculated values into the equation will then give the balanced position, namely, the levitation distance between the electron and the proton at the basic energy level, formulated as

$$d_l = 2.34 \cdot 10^{-11} m. \tag{73}$$
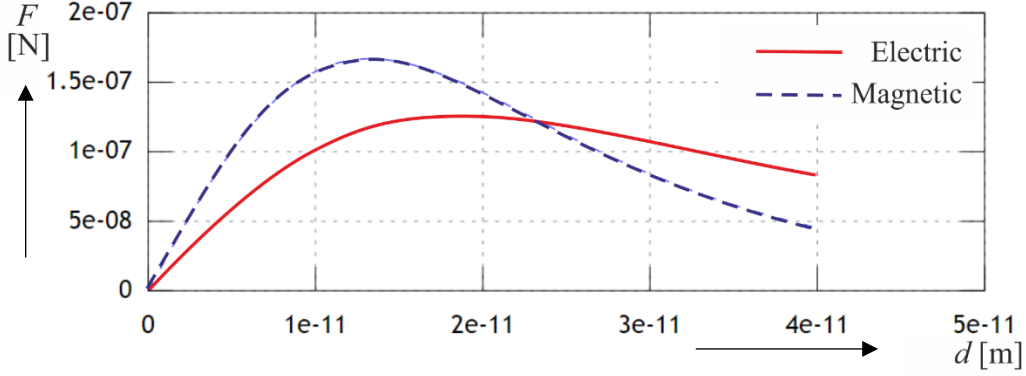
Fig. 57 The forces and levitation distances at the hydrogen atom's basic level.

In the graph that represents the electric and magnetic forces related to the mutual distances (Fig. 59), the intersection of the curves determines the dynamic balance, or levitation.

At the discussed level inside the atom, the energy coupling the proton to the electron (W_v) equals the ionization energy (W_i) required to detach the electron ($W_{v,el}$) from the proton, and it also equals the difference between the energies of the appropriate electric and the magnetic ($W_{v,mag}$) fields. We have

$$W_v = W_i, \tag{74}$$

$$W_i = W_{v,el} - W_{v,mag}. \tag{75}$$

The coupling energy of the electric field is calculated according to

$$W_{v,el} = \frac{q_e^2 \cdot r}{4\pi\varepsilon_0 \cdot r^2}, \tag{76}$$

$$W_{v,el} = \frac{\left(1.6 \cdot 10^{-19}\right)^2}{4\pi \cdot 8.859 \cdot 10^{-12} \cdot 3.5352 \cdot 10^{-11}} = 6.514 \cdot 10^{-18} J, \tag{77}$$

and the formula used for the calculation of the corresponding magnetic field energy is

$$W_{v,mag} = \frac{i_{el} \cdot \mu_0 \cdot \mu_p \cdot r}{4\pi \cdot r^3}, \tag{78}$$

$$W_{v,mag} = \frac{3.85 \cdot 10^{-6} \cdot 4\pi \cdot 10^{-7} \cdot 1.41 \cdot 10^{-26}}{4\pi \cdot \left(3.5352 \cdot 10^{-11}\right)^2} = 4.344 \cdot 10^{-18} \text{J} . \tag{79}$$

Based on Eq. (66), the resulting coupling energy amounts to

$$W_v = 6.514 - 4.344 = 2.17 \, \text{J} = 13.543 \, \text{eV} . \tag{80}$$

The coupling energy of the hydrogen atom is graphically represented in Fig. 60.
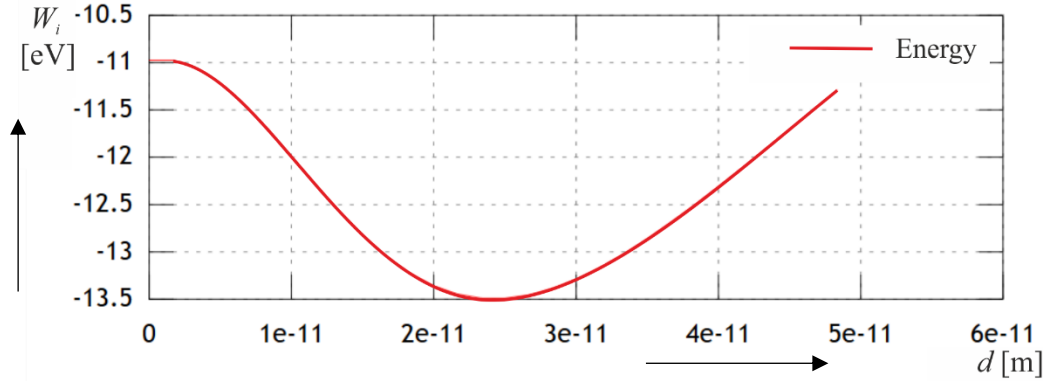

Fig. 58 The coupling energy of the hydrogen atom in relation to the electron - proton distance.

Figure 61 shows the double levitation distance in the hydrogen atom excited up to the second energy level.
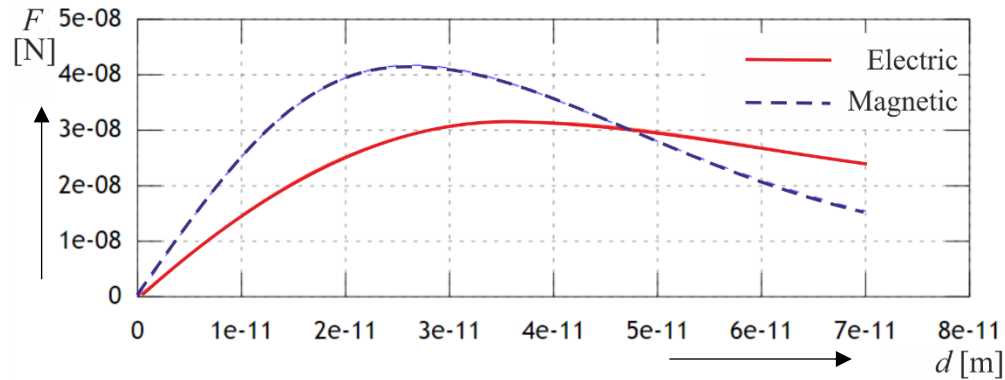
Fig. 59 The distribution of the module of forces in relation to the proton – electron distance, assuming excitation to level *S*2.

5.3   MODEL OF THE DEUTERIUM ATOM

A deuterium atom can be considered a hydrogen atom isotope having a nucleus enriched with one neutron, and the model thus may utilize an electron radius r_e of the same size as that used in the hydrogen atom. Adding a neutron will not change the magnitude of the electric force; in the magnetic force, a magnitude twice as large will be assumed, for simplification. The equation to characterize the balance of the forces will take the form

$$\left\| \boldsymbol{F}_{el} \right\| = 2 \cdot \left\| \boldsymbol{F}_{mg} \right\| . \tag{81}$$
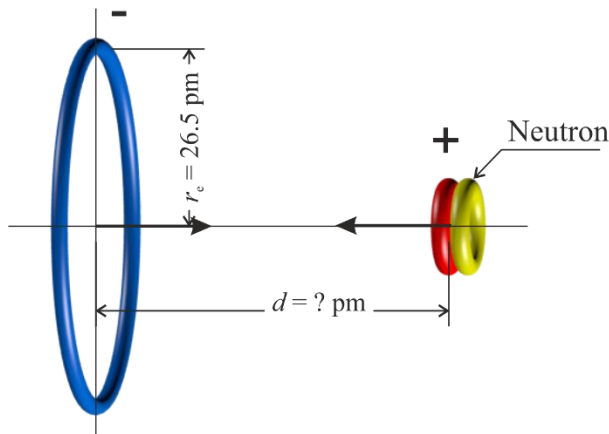
Fig. 60 The RT-based deuterium atom.

An analysis following the hydrogen-related Eq. (72) will yield, for the balanced dynamic state (Fig. 62), the distance between the electron and the proton and therefore also the atom radius; we then have

$$d_{l,D} = 4.2 \cdot 10^{-11} m .$$ (82)
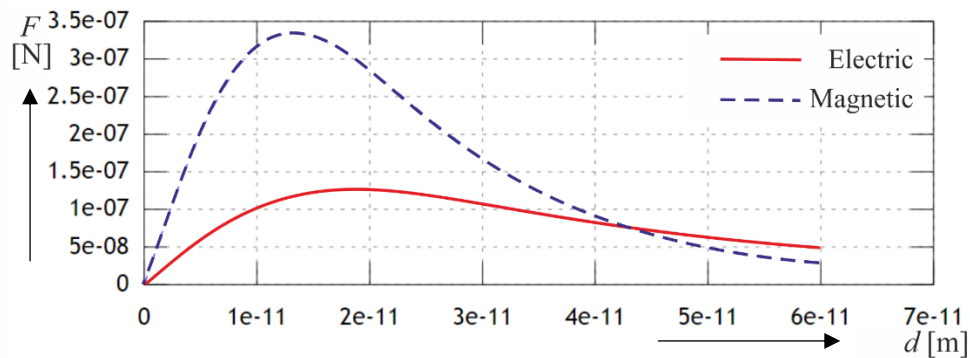
Fig. 61 The modules of the forces and dynamic balance distance in relation to the distances separating the centers of the objects.

5.4   MODEL OF THE TRITIUM ATOM

To set up the designed tritum atom model, we employ the tools and approach from the deuterium modeling procedure, meaning that a neutron is added. The formula to define the dynamic balance and to facilitate distance calculation for the balanced state (Fig. 64) reads

$$\left\| \boldsymbol{F}_{el} \right\| = 3 \cdot \left\| \boldsymbol{F}_{mg} \right\| .$$ (83)
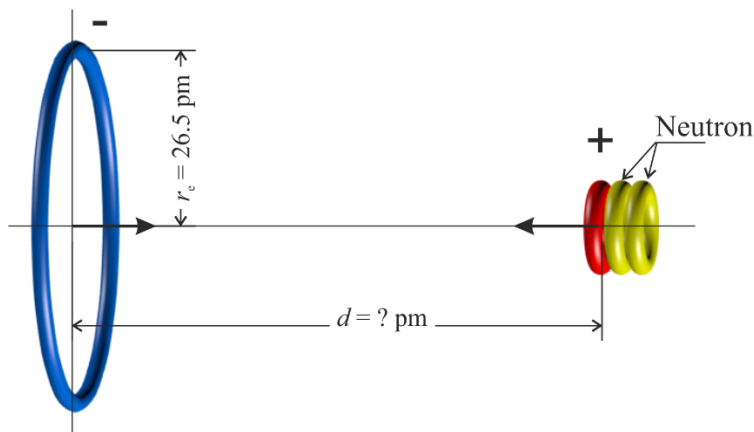
Fig. 62 The tritium atom.

The resulting distance concerning the balanced state and the radius of the tritium atom is

$$d_{l,T} = 5.5 \cdot 10^{-11} m.$$ (84)
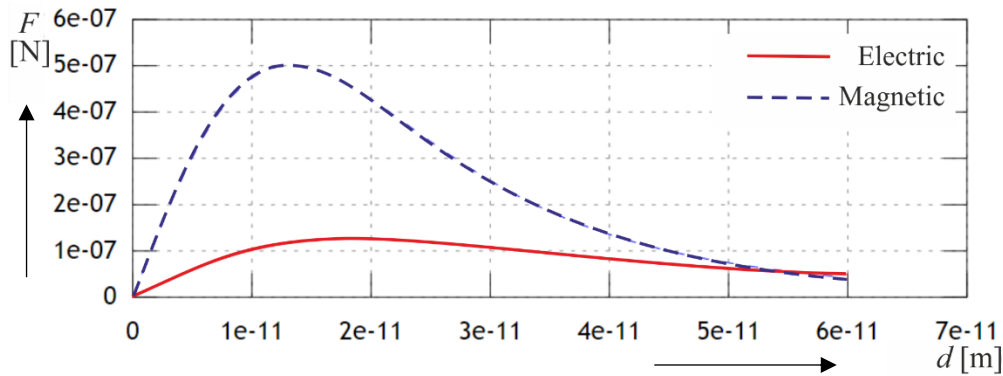
Fig. 63 The patterns of the force modules, and the dynamic balance distance in the tritium atom.

5.5 MODEL OF THE HYDROGEN ION (H₂⁺)
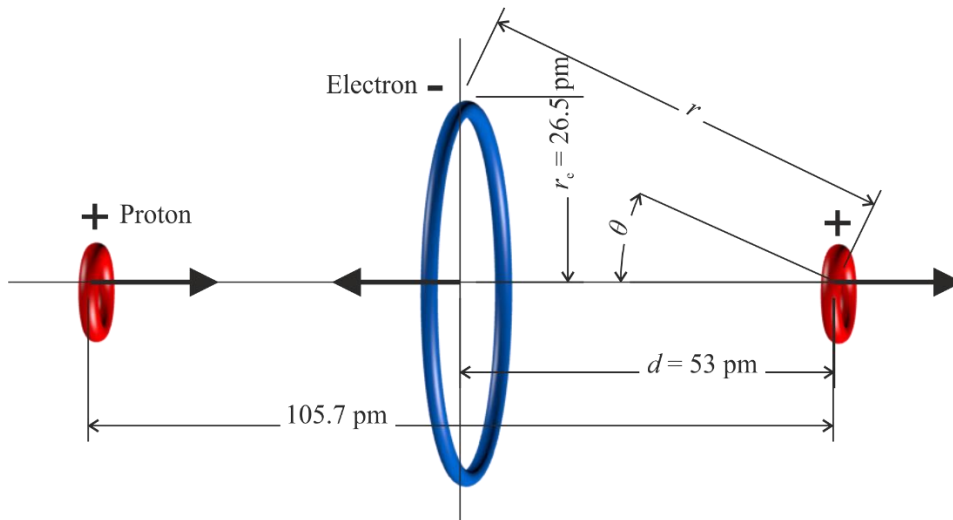
Fig. 64 The modeled hydrogen ion (H₂⁺) and its geometry.

To derive and develop equations to express the dynamic balanced state in the hydrogen ion, we set the distance between the centers of the proton and the electron to $d = 53$pm. The electron's electric charge q_e acting on one proton is selected as half-size, $q_e/2$, because the electric field of the electron has to be divided into two identical parts, symmetrically, in accordance with the transversal plane of the electron ring. The parameters of the electron in the hydrogen atom ion expand through the action of another proton, namely, the radius R_1 increases to twice the size of the radius exhibited by the simple hydrogen atom; such an increase follows from the electromagnetic forces acting in axis y in the plane of the electron. The magnetic field and force will not change even upon variation of a geometrical parameter of the electron, as it will not receive any additional energy in the form of a photon. For the purposes of expressing the electric current, we have

$$i_e = \frac{dq_e}{dt_r};$$ (85)

thus, with the doubling of the radius r_e the electric charge variation time will be reduced by half to maintain identical angular velocity ω. The magnetic flux density

$$\boldsymbol{B} = \frac{i_e \, \mu_0}{2} \frac{\boldsymbol{u}_z}{r_e},$$ (86)

43

will then remain unchanged. The formula to enable setting the balanced dynamic state reads

$$\left\|\frac{2}{2}\cdot F_{el+-} - F_{el++}\right\| = 2\cdot\left\|F_{mg+-}\right\|. \tag{87}$$

The calculated distance relevant for the balanced dynamic state between the centers of the electron and the proton in the hydrogen ion (H_2^+) is specified as

$$d_{l,Hi} = 5.3\cdot10^{-11}m. \tag{88}$$

The patterns of the force modules in relation to the distances between parts of the ion are shown in Fig. 67.
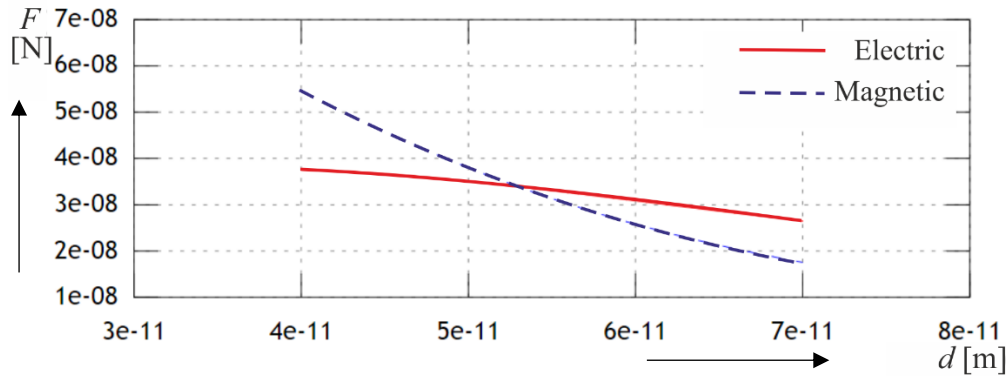
Fig. 65 The force modules and distances characteristic of the dynamic balance in the hydrogen atom ion.

5.6 MODEL OF THE HELIUM ATOM
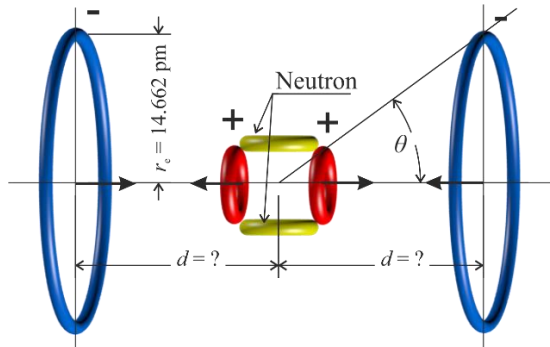
Fig. 66 The developed model and arrangement of the He atom.

The evaluation and quantification of the distance to establish dynamic balance within the helium atom, relating to the electrons (Fig. 68), exploits the dimensional parameters of the rings; the procedure is similar to that used in the electrons that are determined from the term 50.4577 nm by means of Eq. (6) and via the structure of the alpha particle in the helium atom nucleus. The assumed formula for the balanced state of the forces is

$$\left\|F_{el+-}\right\| = 2\left\|F_{mg+-}\right\|, \tag{89}$$

$$d_{l,He} = 3.2\cdot10^{-11}m. \tag{90}$$

This distance applies to both electrons in the model, and it also equals the radius of the He atom (Fig. 69).

44
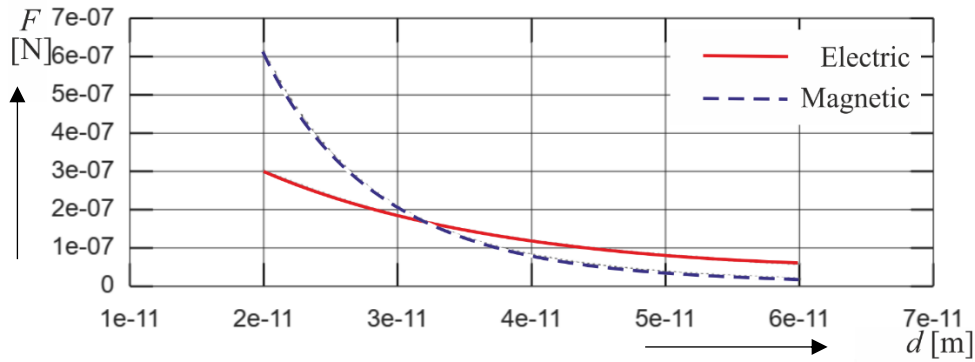
Fig. 67 The force modules and distances characteristic of the dynamic balance in the helium atom.

In the corresponding atom ion (He$_3^+$), the distance to bring the dynamic balance between the sole electron and the nucleus reads $d_{l,He+} = 1.9 \cdot 10^{-11} m$.
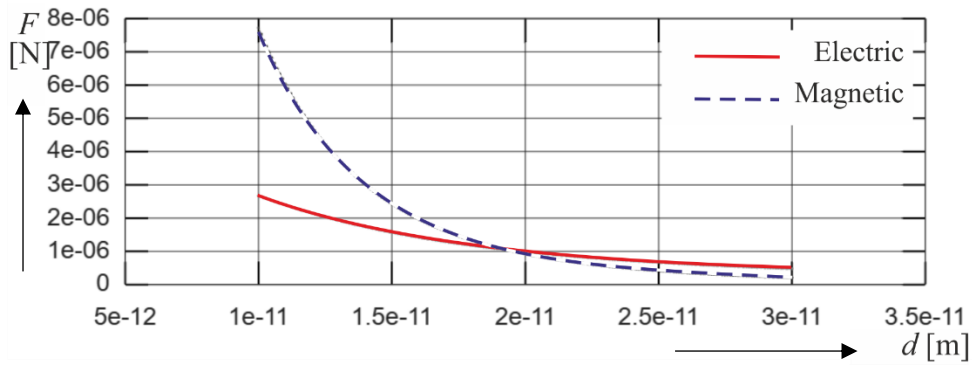
Fig. 68 The patterns of the force modules in relation to the distance concerning the dynamic balance in the helium atom (He$_3^+$).

6 RT-BASED MODELS OF MOLECULES

6.1 COVALENT BONDING

The simplest covalent bonds include, among others, the bond joining the electrons in a hydrogen molecule. In the modeled hydrogen atom, both identically moving electric charges q_e create electrons with parallel spins, Fig. 45. If the electrons are dynamically balanced and geometrically so close to each other that the numerical values of the forces generated by the magnetic and the electric fields are equal, the electrons will couple together through a bond named covalent, Fig. 71.
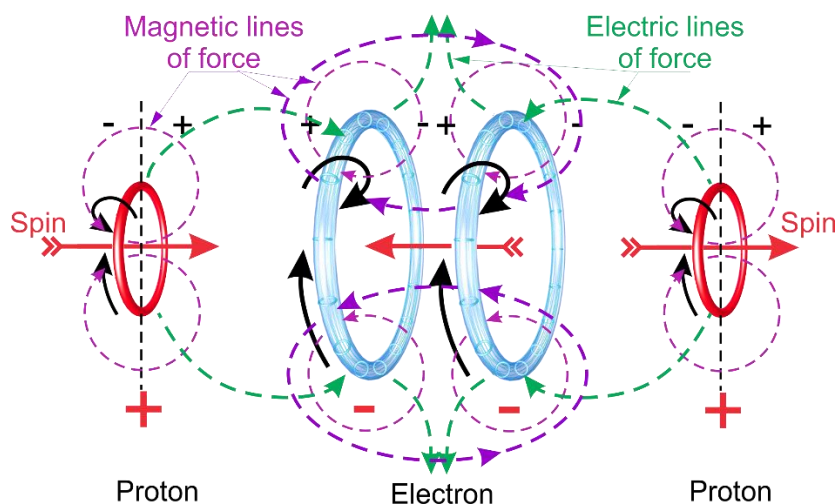
Fig. 69 The schematic distribution of the electrodynamic forces, and the formation of the covalent bond in the modeled hydrogen molecule.

In ring theory, two types of the bond are recognized: σ and π, Fig. 72. Regarding the dynamic balance of the system, the covalent bonds in electrons that have different quantum numbers influence the distances from protons [29].
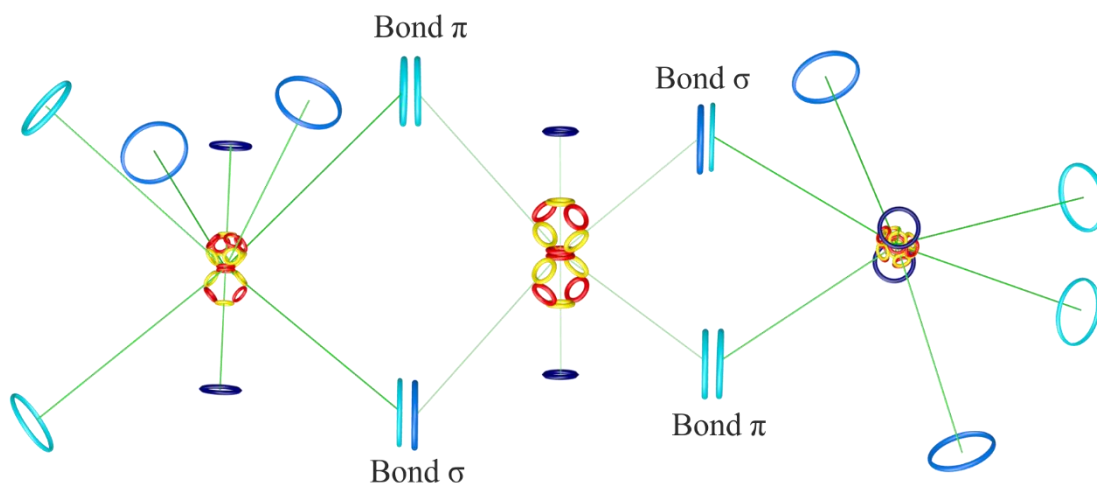
Fig. 70 The types of the covalent bond in a CO_2 molecule.

The modeled carbon atoms, for example, may comprise three bond type combinations: *2s – 2s*, *2s – 2p*, and *2p – 2p*. The *2s* electrons, however, possess different bond energy than the *2p* ones: the ionization energies assumed in the former and the latter then amount to $w_{e,2s}=$ 19.4 eV and $w_{e,2p}=$ 10.6 eV, respectively. This leads us to conclude that the force binding the *2p* electrons to the nucleus

is weaker by almost half than the appropriate force in the *2s* type; such a condition arises from the *2p* electrons having greater internal energy, which is bound to the magnetic component of the electromagnetic field. The prevailing magnetic field components will cause the modeled electron to move away from the nucleus, meaning that the couplings containing the *2p* variant will exhibit a covalent bond in the form of a greater distance between the atomic elements. The basic covalent bond combination *2p* – *2p* takes the size $d = 7.7 \cdot 10^{-11}$ m (Fig. 73); however, in the benzene nucleus bond, *2s* – *2p*, the distance between the centers of the toroidal elements' nuclei is $d = 7.2 \cdot 10^{-11}$ m, Fig. 74.
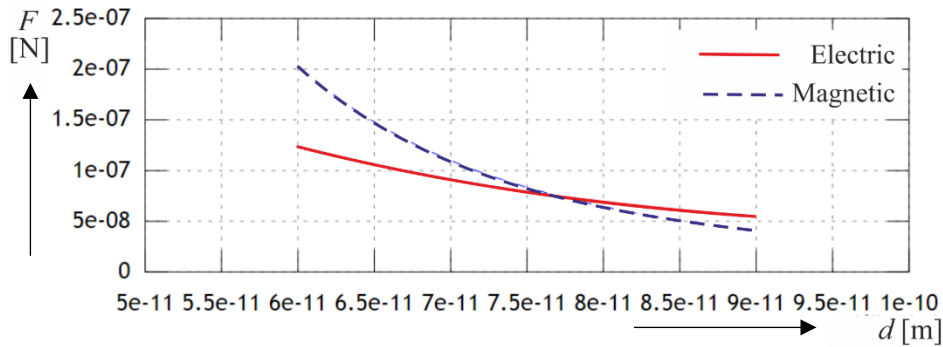
Fig. 71 The distance *d* between the components that create covalent bonds in the carbon atom, *2p-2p*.
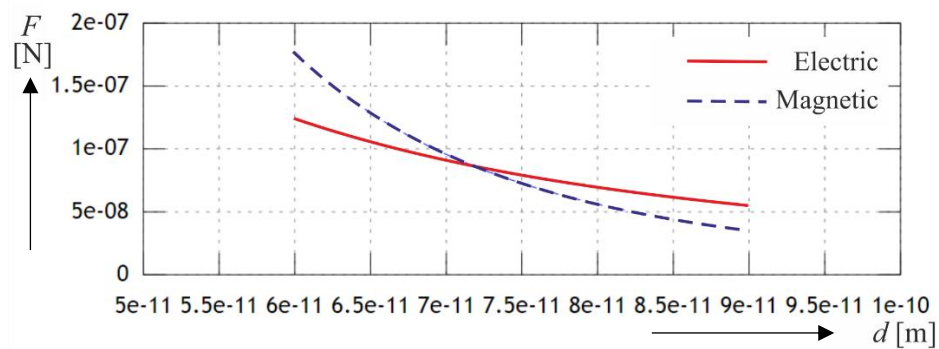
Fig. 72 The distance *d* between the components that create covalent bonds in the carbon atom, *2s-2p*.
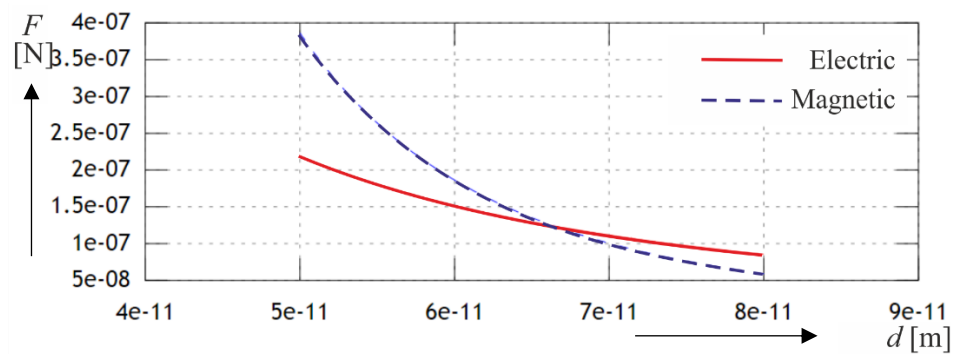
Fig. 73 The distance *d* between the components that create covalent bonds in the oxygen atom.

6.2 MODEL OF THE HYDROGEN MOLECULE (H$_2$)
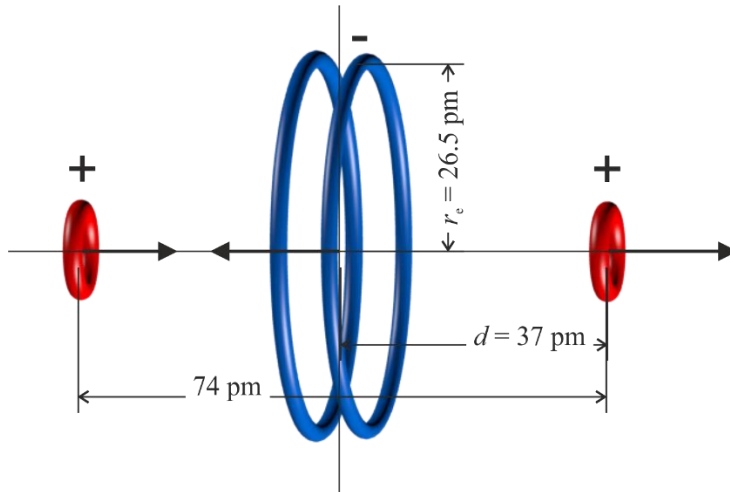
Fig. 74 The modeled hydrogen molecule.

The actual procedure (Fig. 76) can exploit available experimental data relating to the spectral lines, and these data show that the energy of the coupling pair of electrons is located in the first half of the band, between the second and the third energy levels (Fig. 77).
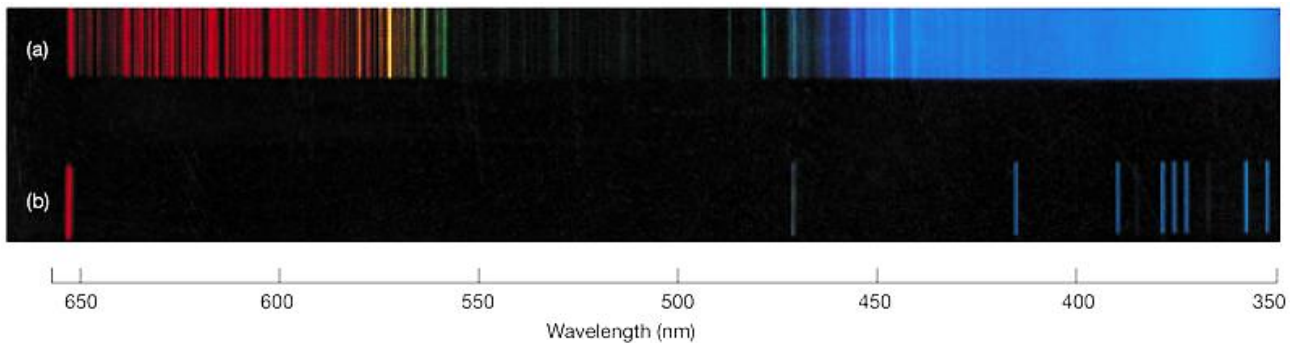

Fig. 75 The experimental spectral data [28]: a) the hydrogen molecule; b) the hydrogen atom.

Within the spectrum, the presence of the region containing multiple lines reveals that the hydrogen atom electrons in the dynamic state, namely, when molecules are formed, emit photons having various energies, with the relevant average value amounting to 2.26 eV. Such a scenario probably results from the emission process taking place at various temperatures T. In molecule-forming atoms, the coupling electrons do not occupy discrete energy levels, as is the case with lone atoms [26].

The spectral lines produced by the release of photons during the electrons' jump to a lower energy level represent photons whose energies are higher than that of the second level. Thus, the modeling and analysis will utilize two electrons, one excited to the *2p* and the other to the *2s* level; in these electrons, hybridization equalized the energies and radii, and the subsequent release of photons caused the magnetic field to vary, in such a manner that the appropriate model would correspond to the first energy level. The radii will remain 2.15 times greater than the basic radius, $r_e = 2.65 \cdot 10^{-11}$ m, due to the impact of the electromagnetic forces acting in the common axis of two opposite ring protons.

The formula capturing the forces to calculate the levitation distance is

$$2F_{el+-} - F_{el++} = 2F_{mg+-}. \tag{91}$$

Assuming optimized distribution of the energies and therefore also different distances d_1 and d_2 between the electrons and the protons, we will have $d_1 = 2.37 \cdot 10^{-11}$ m and $d_2 = 5.04 \cdot 10^{-11}$ m; the

48

total distance between both protons, $d = 7.41 \cdot 10^{-11}$ m, is then identical with the empirically measured one.

The equation of the dynamically balanced forces to define the balanced state in the intertoroidal distance is, based on formula (36), as follows:

$$\left\| 2 \cdot \boldsymbol{F}_{el+-} - \frac{1}{2} \boldsymbol{F}_{el++} \right\| = 2 \cdot \left\| \boldsymbol{F}_{mg+-} \right\|. \tag{92}$$
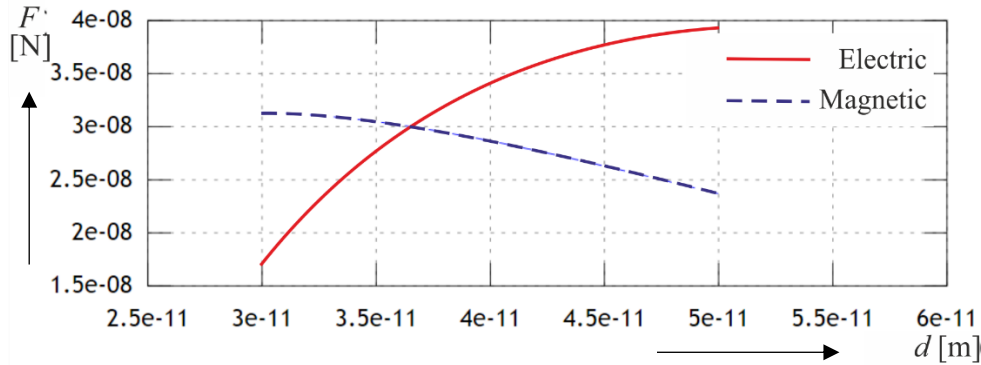
Fig. 76 The patterns of the force modules related to the distance concerning the dynamic balance in the modeled hydrogen molecule.

The quantified distance between the electron and the proton in the balanced dynamic state is

$$d_{lH2mol} = 3.7 \cdot 10^{-11} m. \tag{93}$$

To determine the distance between electrons joined by a covalent bond (Fig. 76), we express the electric and magnetic field forces through the relationship

$$\left\| \boldsymbol{F}_{el} \right\| = \left\| \boldsymbol{F}_{mg} \right\|. \tag{94}$$

The resulting interelectronic distance in the covalent bond corresponds to $3.2 \cdot 10^{-13}$ m.
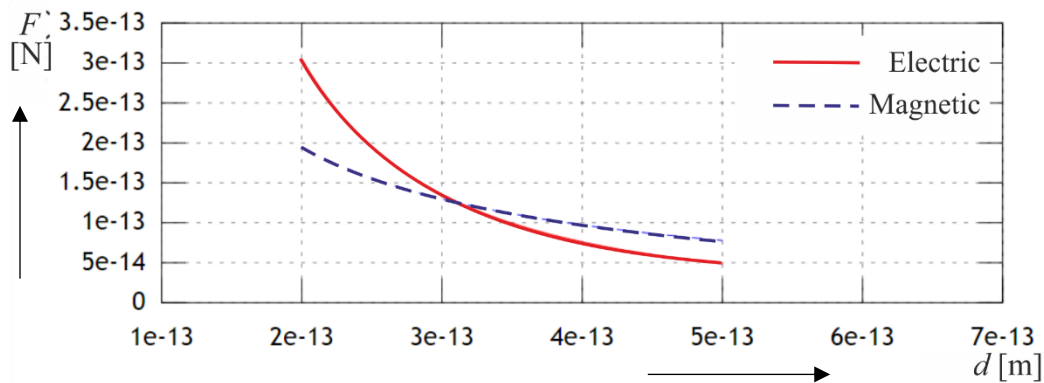
Fig. 77 The patterns of the force modules to determine the balanced dynamic distance between the electrons in the covalent bond.

6.3 MODELING VARIOUS MOLECULES IN RT

The models used to date (for example, that of water) offer several ways of representing the bonds joining the atoms of hydrogen and oxygen, Fig. 80; none of these well-established models, however, explains sufficiently the formation and balanced dynamic state of such bonds, even if the distance and angle between the atoms are known.

Advantageously, using RT to simulate the H_2O molecule has the potential to clarify the positions of the electrons in oxygen atom shells and their bonds with atoms of hydrogen and other elements, Fig. 81.
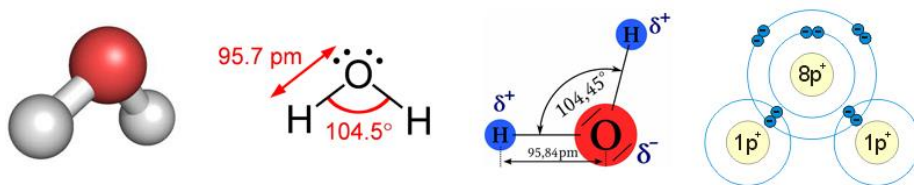

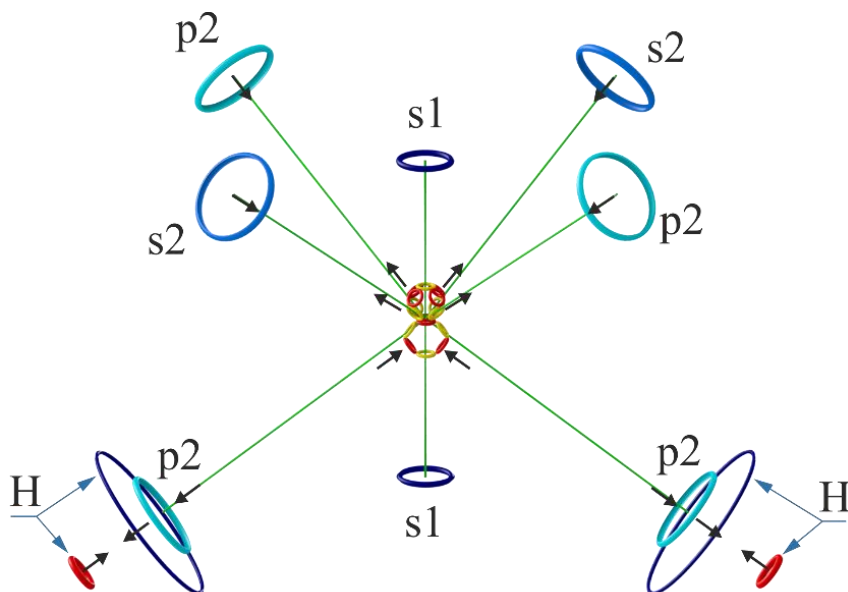**Fig. 78** The classic model and representations of the H_2O molecule.

Fig. 79 The RT-based structure of the H_2O molecule's electron shell.

Supplementary animations are available from website [21]. Similarly, the C_2H_4 (ethene) molecule, Fig. 82, can be used to show that application of RT will enable us to characterize the internal formation and arrangement of molecules explicitly and in detail.
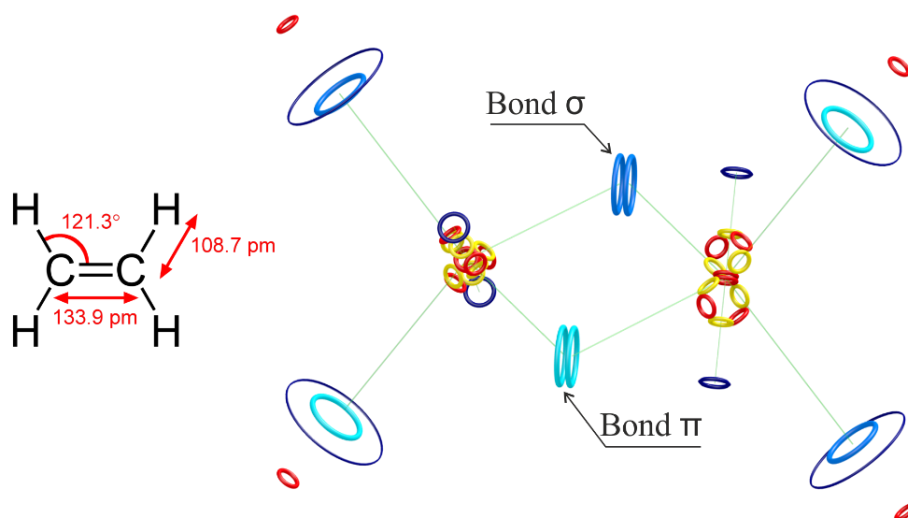
Fig. 80 The modeled C_2H_4 molecule, containing the double interelectronic bond.

Animations illustrating the double bond in carbon are available from website [22].

50

For the purposes of modeling the triple bond between carbon atoms, C_2H_2 (ethyne, or acetylene) embodies a convenient compound because its structure contains three pairs of electrons, Fig. 83.
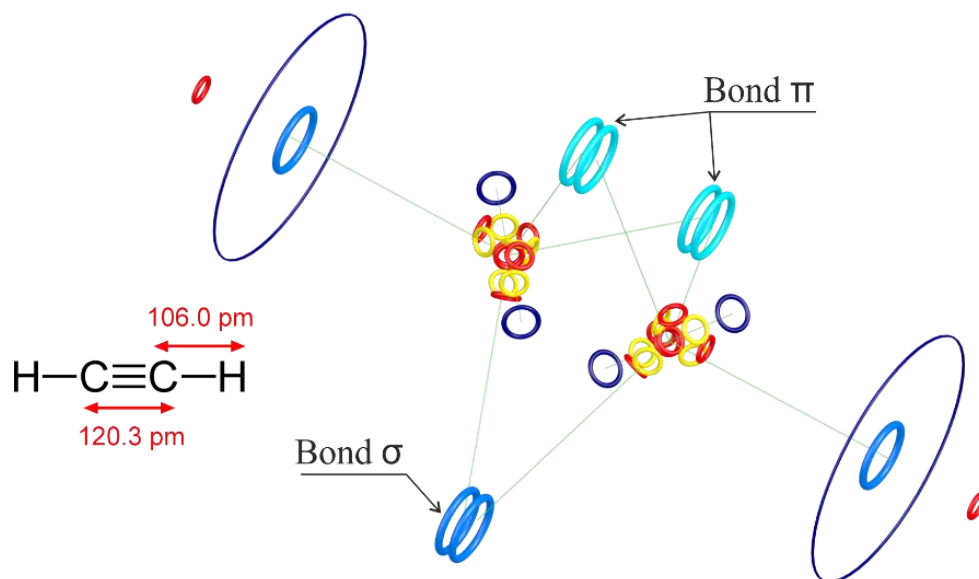

Fig. 81 The RT-based model of the C_2H_2 molecule, indicating the triple bond.

Animations demonstrating the triple atomic bond in carbon are available from website [23]. By utilizing the simulated structure of the carbon nuclei, we yield the structural scheme of a carbyne (Fig. 84), a hypothetical allotropic variant of atoms of polyalkene, $- (C \equiv C)_n -$, where the atoms form long chains of alternating simple and triple bonds.
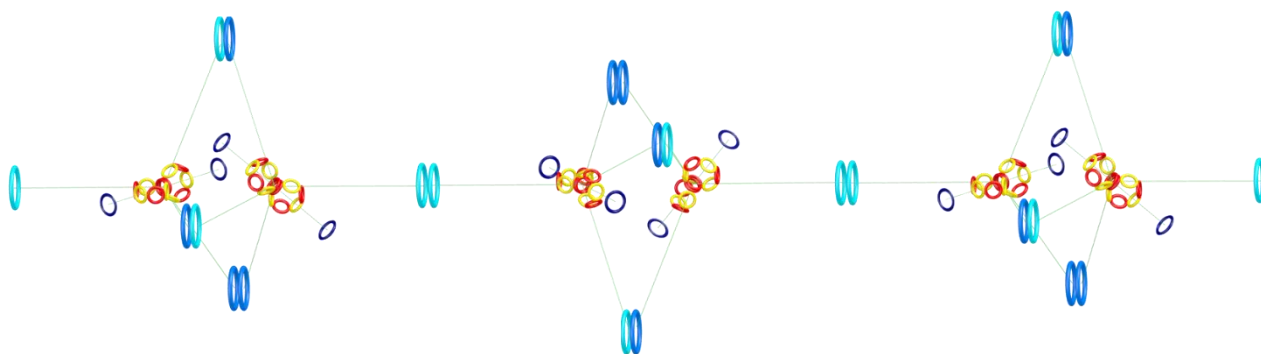

Fig. 82 The model and representation of the linear allotropic structure of a carbyne.

The explicit approach to the modeling can be further illustrated in the hexagon-shaped molecule of benzene, whose vertices host carbon atoms, and each of these is bonded to a hydrogen atom. In the standard, commonly accepted interpretation, electrons are distributed probabilistically throughout the entire nucleus of the molecule; such an arrangement is often represented by a circle inscribed in the hexagon (Fig. 85). None of the classic visualizations, however, displays explicitly the detailed distribution of the elementary particles.
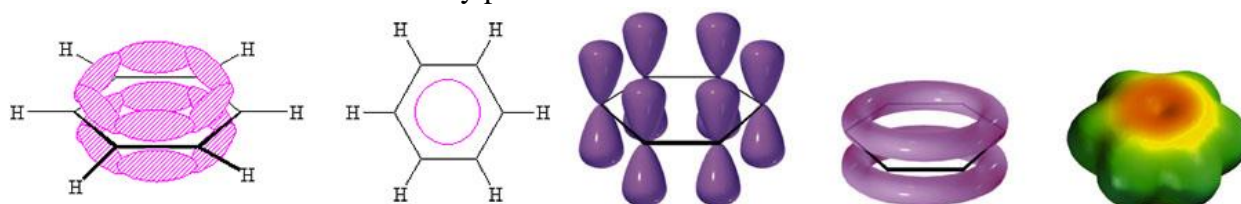

Fig. 83 The structural representations of the benzene molecule.

51

But if we apply the RT-based rings (Fig. 86) to visualize the modeled C_6H_6 molecule, the explicit, exact disposition and variants of the bonds between the individual carbon atoms will be revealed; these bonds nevertheless lack "equality" in terms of the electromagnetic field and dynamic coupling within the structure. The interatomic bond consists of the "s" and "p"-type electrons. The free electrons in the upper part of the modeled molecule have an external spin inverse to that of the electrons in the bottom section; such free electrons are denotable as "delocalized", and with identical spins they can rotate without restriction on the surface of the molecule. The neighboring, coupled hydrogen atoms (or other atoms or groups), too, exhibit an invariably inverse external spin. Interpreting and applying the schematic structure in Fig. 86 allows us to evaluate and explicitly describe bonds with other modeled atoms in the making of more complex molecules and compounds, Fig. 87.

Supplementary animations of the benzene molecule are available from website [24].
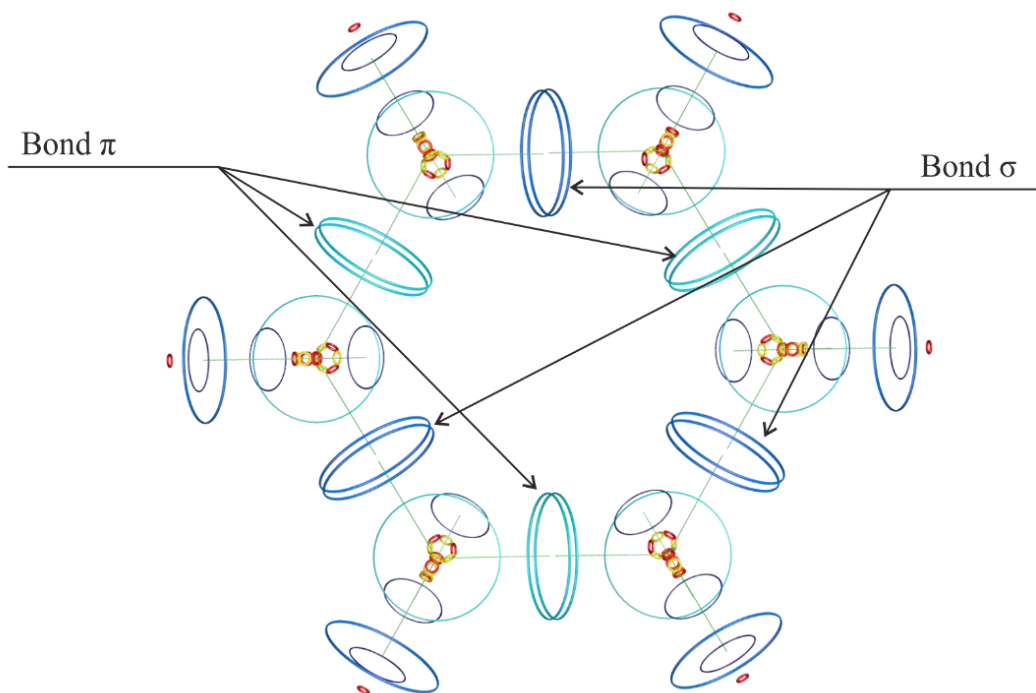

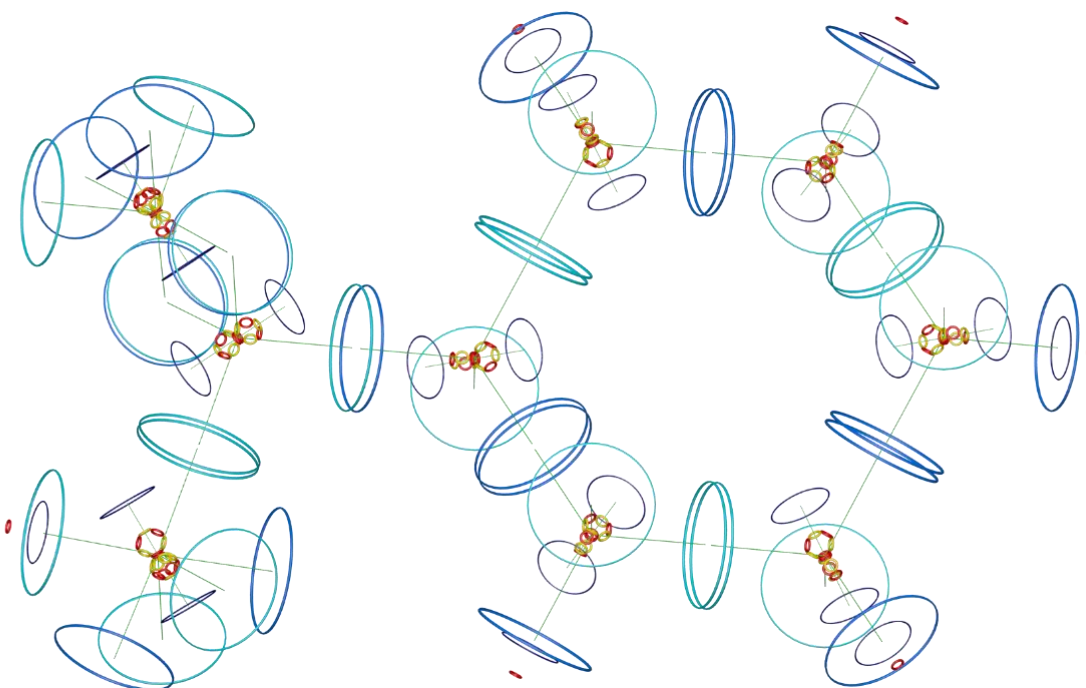**Fig. 84** The RT-modeled structure of the C_6H_6 molecule.

Fig. 85 The 3D structure of the C_6H_5COOH molecule.

If, in the context of the above discussion, RT is employed to model graphene (Fig. 88), the resulting structure may, from the perspective of the spins of the individual carbon atoms (Fig. 50), contain two types of spin coupling and interatomic bond configuration. These two variants, Fig. 89, alternate regularly, and the structure cannot be formed from only one of them (Fig. 90). Analyzing the model via RT could influence several relevant aspects, including the rational setup of nanoparticles; explicit description of the properties; replacing a bond type or group with another one, large or small; or substituting another element for the carbon.

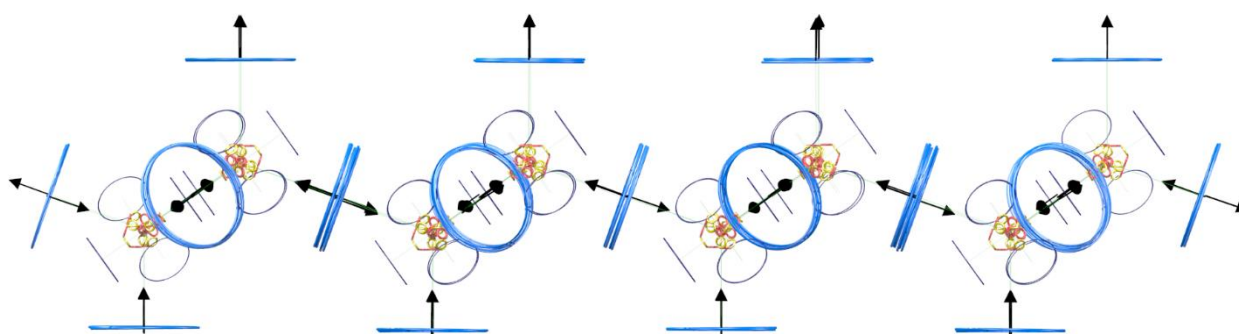Supplementary animations of the graphene model are available from website [25].

Fig. 86 The structure of graphene, and the electron spin orientation. The location of the outer electrons on parallel axes in a given direction brings the maximum achievable conductivity of graphene: after being excited, the electrons move away from the protons. Due to the impact of the external magnetic field, the electrons' motion is smooth, exploiting an optimum gyroscopic arrangement.
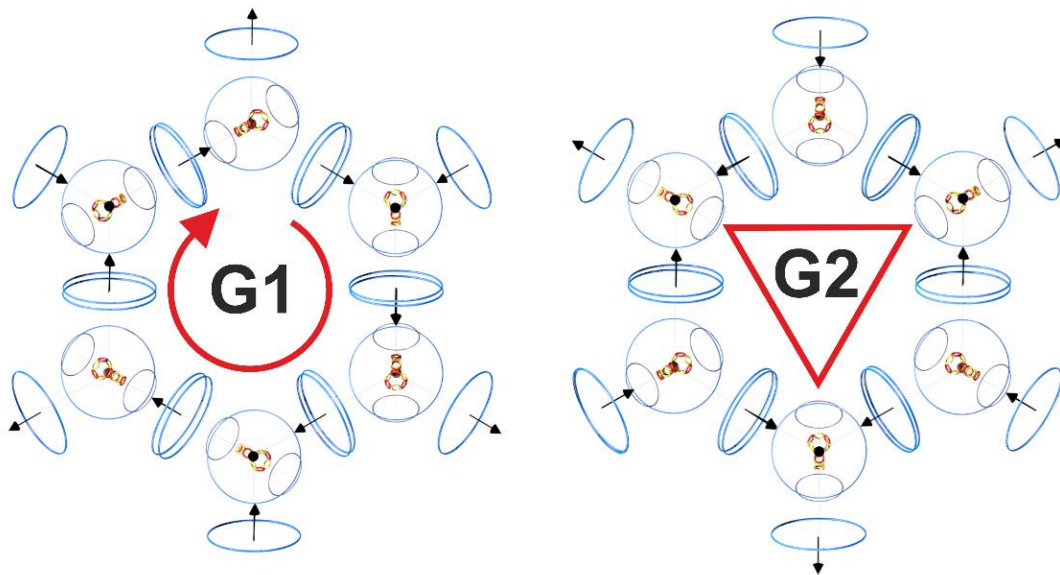
Fig. 87 The interatomic bond configurations in graphene, as related to the spin coupling.
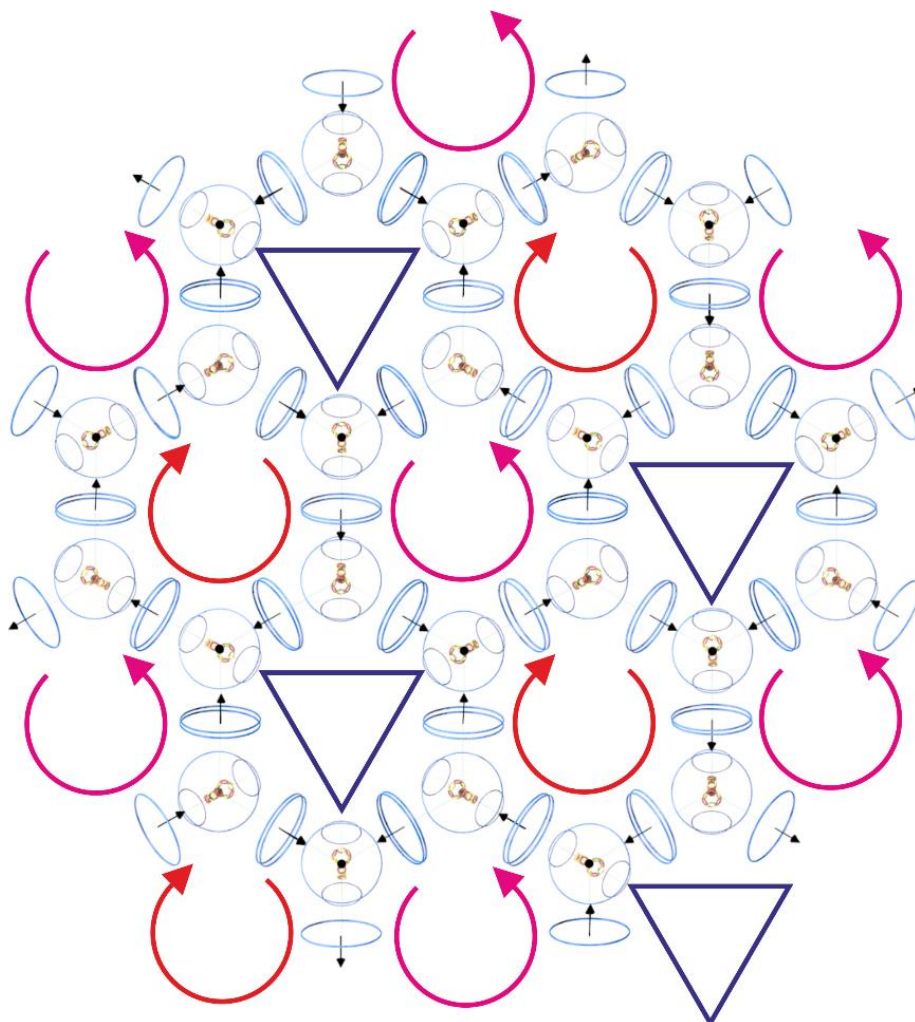

Fig. 88 The arrangement of components in graphene according to the spin coupling type.

7 CONCLUSION

Modeling fudamental components of matter by means of RT embodies an explicit approach to the analysis and simulation of elementary structures. Within such a concept, atomic nuclei, atoms, and molecules can be simulated and their properties predicted more easily than possible via the standard implicit methods, which rely on stochastic models and analyses. The basic ring theory does not require the complex mathematics of discontinous processes and stochastic techniques, and thus is very simple; the understanding and effective usability of RT are conveniently supported by graphical representations of the examined structures. Importantly in this context, the entire theory has been formulated upon well-known interpretations of the electromagnetic field and electrodynamics.

In terms of its potential, RT may contribute towards clarifying diverse problems of atomic, particle, and molecular physics (such as the reasons for the stability and reactivity of atoms and molecules) and nanoengineering, namely, effects difficult to explain through implicit description. The partial ideas and hypotheses may also influence the basics of particle chemistry and physics.

Modeling and characterizing in an explicit manner the behavior of elementary components of matter, including protons, neutrons, and electrons, substantially enriches rational particle engineering and, by extension, the nano-domain; the approach thus prospectively could enable us to design and verify new molecules and materials with specific properties, via standard models applied to demonstrate laws and processes that to date may have appeared problematic to interpret.

7.1 ACKNOWLEDGEMENT

7.2 REFERENCES

[1] Feynman RP. (1986), *Elementary Particles and the Laws of Physics.* The Dirac MemorialLectures, Cambridge University Press, Cambridge; (1987).

[2] Landau, Lev Davidovič. - Haan-Gruiten. (2014), *Klassische Feldtheorie*, Verl. Europa-Lehrmittel Nourney, Vollmer, 2014, unveränd. Nachdr. der 12., überarb. Aufl., 4. Dr.

[3] Bohr N. (1913) *Phil Mag*. 1913; 26:1.

[4] Schrödinger E. (1930), *Über die kräftefreie Bewegung in der relativistischen Quantenmechanik*, Berliner Ber; 1930:418.

[5] Schrödinger E. (1931), *Zur Quantendynamik des Elektrons*, Berliner Ber; 1931:63.

[6] http://www.lanl.gov/discover/news-release-archive/2016/index.php

[7] Sklenar J., et al. (2016), *Perspective: Interface generation of spin-orbit torques*, Journal of Applied Physics 120, 180901 (2016); doi: http://dx.doi.org/10.1063/1.4967391,

[8] Braibant, S., Giacomelli, G., Spurio, M. (2012), *Particles and Fundamental Interactions*, An Introduction to Particle Physics, 2nd, Springer, 1–3., pp. 457 2012

[9] Viceconti, M. (2012), *Multiscale Modeling of the Skeletal system*, Cambridge University Press, UK, pp. 210 ,2012

[10] E. V. Anslyn, D. A. Dougherty (2005), *Modern Physical Organic Chemistry*. University Science Books, Kausalito, California 2005. ISBN 1-891389-9

[11] Ošmera P. (2009), *The Vortex – ring - fractal Structure of Hydrogen Atom*, in Proceedings of WCECS2009, San Francisco, USA, pp.89-94., October 20-22, 2009

[12] Osmera, P. (2006), *Chaotic system with vortex- fractal structures*. In Proceedings of 13th Zittau East – West Fuzzy Colloquium. ISBN: 3-9808089-8-X, pp. 182, 2006.

[13] Osmera, P., Werner,P. and Osmera,P. jun., 2015, *Ring structures of atoms and molecules*. In Roychoudhuri, C; Kracklauer, A; DeRaedt, H. *Proceedings of SPIE : Nature of Light : What are Photons? VI*. Bellingham: SPIE, 2015. pp. 1-15, 15 p. ISBN 978-1-62841-736-4. doi:10.1117/12.2207303.

[14] Fiala, P. (2016), *Studie vlastností základního stavebního elementu hmoty v souvislosti s modelováním a topologickým pojetím fyziky a elektrohydrodynamiky*, Výzkumná zpráva III/16, Ústav teoretické a experimentální elektrotechniky FEKT VUT BRNO, Laboratoř modelování a optimalizace v elektromechanických systémech FEKT VUT v Brně, str.34, 04.2016 (*Investigating the Properties of the Basic Element of Matter in relation to Modeling and Topological Physics and Electrodynamics*. Research report no. III/1, the Department of Theoretical and Experimental Electrical Engineering, FEEC, BUT).

[15] Savolainen, J., Uhlig, F., Ahmed, S. Hamm, P. and Jungwirth, P. (2014) *Direct observation of the collapse of the delocalized excess electron in water*, Nature Chemistry 6, 697–701 (2014) doi:10.1038/nchem.1995. Received 19 December 2013 Accepted 04 June 2013 Published online 06 July 2014.

[16] J. J. Mestayer, (2008): *Realization of Localized Bohr-Like Wave Packets*; Phys. Rev. Lett. 100, 243004 (2008)

[17] Rice University Press Release, (2008): *Physicists create millimeter-sized "Bohr atom"*, 2008

[18] Williamson, J.G. & van der Mark, M.B. (1997): *Is the electron a photon with toroidal topology?* Annales de la Fondation Louis de Broglie, volume 22, no.2, 133 (1997).

[19] https://www.photonics.com/Article.aspx?AID=52250

[20] http://youtu.be/wX7vy9dZ724

[21] https://youtu.be/MdciqalsJOc

[22] https://youtu.be/VxdtUEwTg1Y

[23] https://youtu.be/mbnFIHiKK1k

[24] https://youtu.be/zgzenuQqp0w

[25]. https://youtu.be/Dfozb1LshEw

[26] Kanarev Ph.M., (2005): *Foundations of Physchemistry of the Microworld.* The sixth edition. 500 pages. Redacted.

[27] NIST Atomic Spectra Database Lines Form: https://www.nist.gov/pml/atomic-spectra-database

[28] http://pages.uoregon.edu/jimbrau/BrauImNew/Chap04/FG04_14.jpg

[29] KOTLÍK, B., (2009): *Chemie I, II v kostce pro střední školy*. Praha: Fragment, 2009. (*High School Chemistry in a Nutshell, I and II*. Praha: Fragment, 2009*).*